Exponent
Failure Analysis Associates®

Exponent
310 Montgomery Street
Alexandria, VA 22314

telephone 703-549-9565
facsimile 703-549-4225
www.exponent.com

Metallurgical Evaluation Of DOT E6498-2216 Aluminum Gas Cylinder – T119168

Prepared by:

Timothy R. Smith, Ph.D., P.E.
Carol E. Moyer

08/30/99

Project No.: DC18234.000
QA ID No.: DC18234.000/C0F0/0899/TS03

TABLE OF CONTENTS

LIST OF FIGURES

Executive Summary

The remains of a US-DOT-E6498-2216 type aluminum gas cylinder manufactured by Luxfer USA were subjected to metallurgical evaluation. The cylinder was reported to have failed catastrophically during filling. The cylinder was found to meet the chemical and mechanical property requirements applicable at the time of its manufacture. Folds, or cusps, up to 0.040 inches (1 mm) deep were found at the inside of the cylinder neck, and branching cracks extended from some of these folds. The failure of the cylinder resulted from cracks that initiated at such neck folds and that gradually propagated by sustained load cracking (SLC). Fractography established an SLC crack path through the cylinder wall, consistent with reports that the cylinder was leaking prior to rupture. An estimate of the time-to-rupture indicates that a crack existed in the neck region for at least 8 years prior to rupture.

1.0 Introduction

Luxfer Gas Cylinders, a subsidiary of Luxfer, Inc., contracted with Exponent Failure Analysis Associates (FaAA) to perform a metallurgical examination of the remains of an aluminum gas cylinder. The cylinder was a US-DOT-E6498-2216 type, manufactured by Luxfer USA. It was used in a Scott Air-Pak SCBA and was recovered from service in Summerfield, NC. FaAA was informed by Luxfer that the rupture of the cylinder occurred during a pressure fill process and that the cylinder was reported to have been audibly leaking during the fill process. The fragments of the cylinder and regulator were provided to FaAA for analysis.

The scope of this investigation was to perform a detailed evaluation of the cylinder remains, including photodocumentation and non-destructive examinations, chemical analysis, tensile testing, metallographic sectioning, and fractography. In addition, an attempt was made to quantify the length of the largest crack(s) in the cylinder at the time of final rupture, to determine the mechanism(s) of crack growth, to determine if the cylinder was leaking prior to rupture, and to estimate the time frame for the crack(s) to grow. This report presents the findings of this evaluation.

2.0 Visual Examination

A visual examination of the provided cylinder fragments was performed. The fragments are shown in the as-received condition in Figure 1. The cylinder separated into three fragments. The piece labeled 1A spanned approximately half of the cylinder at the neck, with two flat fracture surfaces along a diameter, then tapered to a small width just above the cylinder bottom. Fragment 2A comprised the balance of the cylinder side-wall. The circular, slightly domed bottom of the cylinder was labeled 3A. The valve assembly from the cylinder was also recovered, and was designated 4A.

Stampings on the exterior of the neck indicate that the cylinder was manufactured by Luxfer USA, per the DOT E6498 exemption[1] and its serial number was T-119168, Figure 2 [2]. The first hydrostatic test on the cylinder, also indicated by stampings, was performed in June 1977. This was taken as its date of manufacture. Other inspection stampings indicated that the cylinder had been pressure re-tested on 1/84, 2/89, 9/93 and 10/98, as shown in Figure 2. Neck stampings and a decal on the side of the cylinder identified its rated pressure as 2216 psi.

In the neck region, the fracture surfaces of the cylinder fragments were flat and approximately coincident with the cylinder radial-axial plane (Figure 3). In the regions away from the cylinder neck, the fracture surfaces were inclined to the radial direction, with features consistent with shear fracture. Figure 3(b) shows one of the fracture surfaces in the neck region. Beach marks[3] appear to be emanating from near the bottom of the threaded hole. The recovered fragments had sustained some impact damage, presumably all as a result of the rupture event, on both the fracture surfaces and on the cylinder exterior. Remains of yellow paint were visible over the outside of the cylinder. Traces of other colors of paint and other contaminants were found on the cylinder fragments and on the fracture surfaces. These materials were not further identified.

The inside wall of the cylinder in the neck region showed multiple folds (or cusps) from the original manufacturing process (see Figures 4 and 5). Two orientations of folds were noted. The predominant ones were along the axis of the cylinder; however a second set of shallow folds oriented circumferentially were also present, Figure 4. A small crack was observed to extend from one of the folds across the lowest thread in the neck, as shown in Figure 5. Also notable in this figure is the absence of deposits in the inlet hole threads. Some deformation in the threads was noted, particularly in the lowest threads. The inside surface of the cylinder was generally uniform in color, and no evidence of corrosion was visually observed.

3.0 Quantitative Chemical Analysis

Samples of chips of the cylinder alloy were taken from the neck using an electric drill. These chips were dissolved in solution and analyzed by atomic absorption spectrometry to determine their chemical composition.

The results of this analysis are shown in Table 1 and indicate that the cylinder conforms to the Aluminum Association (AA) 6351 alloy specification and satisfies the DOT-E6498

[1] DOT E6498 is an exemption, dated 7/76, to the provisions of DOT's then-applicable Hazardous Materials Regulations granted to Luxfer, USA Ltd. to manufacture, mark and sell cylinders for the use in transportation in commerce of certain liquefied and nonliquefied compressed gases. This exemption satisfies the DOT-3AL section of 49 CFR-178.45.

[2] The 49 CFR 173.23(c) section dealing with Previously Authorized Packaging requires that cylinders manufactured under the E6498 exemption be stamped with the specification identification "3AL" before or at the next retest after July 2, 1982. The as-received cylinder pieces did not show this stamping.

[3] Beach markings are indicative of progressive crack growth and can be related to changes in load conditions.

specification for aluminum alloy chemistry. These results also show compliance with the current US-DOT federal regulation 49 CFR 178.46(b). Note that the lead (Pb) level found was below the detection threshold of 50 weight-ppm (6.5 atomic-ppm[4]) for the sample size provided for chemical testing. In addition, the bismuth (Bi) level was below 50 weight-ppm (6.5 atomic-ppm).

Table 1: Chemistry of the Cylinder

Element	Composition (wt. %)	
	Test Result Neck	DOT-E6498 Specification
Mg	**0.62**	**0.40-0.80**
Si	**1.00**	**0.70-1.30**
Ti	**<0.02**	**0.20 max**
Mn	**0.53**	**0.40-0.80**
Fe	**0.28**	**0.50 max**
Cu	**0.02**	**0.10 max**
Zn	**<0.02**	**0.20 max**
Bi	**<0.005**	**0.01 max**
Pb	**<0.005**	**0.01 max**
Al	**Balance**	**Balance**

Chemical composition determined by atomic absorption spectrometry in accordance with the ASTM-E663 and ASTM-D3335 standards.

4.0 Mechanical Testing

4.1 Tensile Testing

Full thickness tensile test coupons were cut from the cylinder wall, aligned approximately along the cylinder axis, Figure 6. Some difficulty was experienced in obtaining suitable specimens due to the nature of the deformation induced to the remains during the rupture event. Suitable coupons were obtained, however, and were tested at room temperature in accordance with ASTM B-557 and following the procedure given by 49 CFR 178.46(i)[5]. The results of these tests are shown in Table 2.

[4] Calculated using the equation: atomic-ppm (Pb) = weight-ppm (Pb)*GMW(Al)/GMW(Pb); where GMW is the gram molecular weight of the element in parenthesis. The same equation was used for the bismuth level with Bi replacing Pb.

[5] The DOT 3AL specification requires tensile test specimens to be taken in pairs oriented 180 degrees apart. In these tests, two specimens were adjacent to one another, while one was sectioned from material about 90 degrees away, in order to preserve as much of the cylinder remains as possible. The balance of the procedure followed 49 CFR 178.46-(i)-98.

Table 2: Tensile Properties

Test	Yield (ksi)	UTS (ksi)	Elongation (%)
T-1	45.6	51.5	16
T-2	44.3	51.5	14
T-3	47.1	52.0	16
Average	45.7	51.7	15.3
49 CFR 178.46(b) minimum values	37.0	42.0	14

Tensile tests confirmed properties consistent with AA6351 material in the T6 temper condition [1]. DOT E6498 requires that the material be AA6351-T6, with minimum tensile elongation of 14%. The test results also met the minimum property requirements of 49CFR 178.46(b).

4.2 Hardness Testing

A slice of material was removed from the neck region of the cylinder, designated specimen 1A-3, shown in Figure 7. A total of ten Rockwell B hardness (HRB) measurements were made on this slice, using a Leco RT-370 Rockwell hardness tester. The results are shown in Table 3. The typical hardness of AA6351 material in the T6 temper has been reported to be 95 BH (Brinell), which is equivalent to about 56 HRB[6]. No significant difference in hardness was observed between the area adjacent to the neck threads and an area approximately two inches away from the threads.

Table 3: Hardness Measurements

Component	Indent No.	Hardness (Rockwell B)	Average Hardness (Rockwell B)
	1	62.3	
Section 1A-3	2	64.3	
Near neck	3	63.7	63.5
threads	4	64.1	
	5	63.3	
	6	61.8	
Section 1A-3	7	62.8	
Away from	8	63.2	63.1
neck threads	9	63.8	
	10	64.1	

[6] Hardness numbers were converted using a table published by ASTM in Standard E 140-97 [2].

5.0 Sectioning and Metallography

Sections cut from cylinder fragment 1A are shown in Figure 7. Two wafer sections of the fracture surface, one on each side of the inlet hole, were cut such that the flat-faced portion of the fracture surface was separated from the parent fragment. These wafers were labeled 1A-1 and 1A-2 and were used for optical and scanning electron fractography. An additional section, labeled 1A-3, was cut from the cylinder neck behind 1A-2 and was used for both hardness measurements and metallography.

Section 1A-3 from the neck region was metallographically polished and etched, as shown in Figure 8. The microstructure, as shown in Figures 8 and 9, was typical of AA6351 material in the T6 temper condition [3,4]. The grains, in general, were very elongated (i.e., with an aspect ratio > 1). The grains along the sidewall of the cylinder were significantly smaller and less elongated than those in the thickest section near the neck.

A series of cracks extended from the interior surface of the cylinder, as shown in Figure 10. The cracks appeared to emanate from small circumferentially-oriented folds on the inside cylinder wall. The cracks were branched and appeared to preferentially follow the lighter-etching regions of the microstructure.

A second microstructure sample, 2A-1, was prepared perpendicular to the cylinder neck axis, a shown in Figure 11(a). Examination of this specimen confirmed branching cracks extending from axially-oriented folds around the circumference of the neck, Figure 11. Several other cracks were observed in the same specimen, running approximately parallel to a flat-faced fracture surface, as shown in Figure 12.

The cylinder threads were found to be in good condition (other than the deformation previously noted), and visual examination found them to be free of corrosion.

6.0 Fractography

Both of the sections containing the flat-faced fracture surfaces shown in Figure 3 (section 1A-2) were examined optically and in the scanning electron microscope (SEM). The optical examination revealed that, in both cases, the flat-faced region of the fracture surface showed little macroscopic ductility. Just outside of this region, the fracture surface transitioned to an inclined shear-type of fracture.

Fractographic analysis showed several beach marks (see Figures 3 and 14) indicating progressive crack growth in the flat-faced region. The fracture surface appearance at various locations was documented in a systematic manner. A series of SEM fractographs taken of the fracture surfaces is presented in Figures 13 - 17. SEM fractography revealed that fracture surface 1A-1 exhibited features very comparable to 1A-2.

A significant fold was observed to intersect each fracture surface along the inside surface of the cylinder, near the base of the cylinder neck (Figure 3(b)). The fold was

approximately 0.040 inches (1 mm) deep on fracture 1A-2. On fracture surface 1A-1, a similar neck fold at the edge of the fracture surface was about 0.008 inches (0.2 mm) deep. EDS analysis of a fold surface showed the presence of a chromium-containing coating, similar to that found on the cylinder ID, indicating that the fold had been present from the time of manufacture.

The area of the fracture surface near the neck fold in 1A-1 is shown in Figure 13. Near this fold, the fracture surface was flat, with fine scale features consisting of incompletely formed dimples and round, shallow holes. Although predominantly flat, the fracture surface did contain steps (reflecting the local grain size, see Figure 8), indicating that the cracking was intergranular. Similar flat fracture with microdimpling extended from the base of the neck (Figure 13) to the top of the inlet hole (Figure 15).

Fractographs in the region of a defined beach mark are shown in Figure14. At location (b), the beach mark itself was observed to contain clearly defined dimples, suggestive of ductile fracture. Inside the beach mark at (a), the fracture surface was predominantly flat and intergranular, with very shallow or incompletely formed dimples, with a mixture of more ductile dimpled features. Outside the beach mark, at location (c), the fracture is similar to (a), but with larger dimples and a higher fraction of ductile regions. Based upon these observed features, the beach marks are believed to indicate an interruption in low ductility progressive cracking, which then resumed until the crack reached a critical length at a subsequent crack length. Outside the second defined beach mark, the fracture was observed to transition abruptly to shear fracture features, consisting of well-formed, elongated dimples.

Tensile overload fracture in AA6351-T6 cylinder material has been shown to produce ductile dimpled rupture features, including both macro- and micro-dimples [3]. In addition, portions of a tensile fracture surface commonly include intergranular fracture features, with well-formed microdimpling on the facets. The flat-faced fracture surface of fragment 1A-2 showed low ductility intergranular fracture (i.e., with incompletely formed microdimples) combined with varying degrees of dimpled rupture. The appearance of the fracture surface from the second defined beach mark outward was predominantly consistent with ductile rupture. The concentration of ductile features, intermixed with low ductility areas, increased in the directions away from the threaded inlet hole.

Near the outer surface of the cylinder neck, the fracture surface was again predominantly low ductility intergranular, with shallow holes and micro-dimples visible on the fracture surface. As the crack approached the outer surface, the fraction of ductile features increased. Figures 16 and 17 depict two areas in which "fingers" of low-ductility fracture were found to extend to the cylinder outside surface. The distance along the outer surface from Figure 16 to Figure 17 was approximately 1/4 inch.

7.0 Discussion

Examination and testing of the subject cylinder material demonstrates that it meets the chemical and mechanical property requirements of DOT E6498 and DOT 3AL in the current edition of 49 CFR 178.46. The composition of the alloy complies with the Aluminum Association specification for AA6351 and also meets the chemical limits specified in 49 CFR 178.46 for both lead (Pb) and bismuth (Bi). The tensile test results and hardness measurements indicate that the material meets the T6 temper mechanical properties, in accordance with DOT E6498 and DOT 3AL. The microstructure appears to be typical for this alloy and heat treatment.

Examination of the cylinder remains suggests that the rupture of the cylinder originated from the neck region below the threads and near the base of the inlet hole. The flat-faced, radial fracture occurred at the neck region with little macroscopic ductility, followed by transition to an inclined (i.e., non-radial) shear-type of fast fracture. Each of the flat-faced fracture surfaces observed among the cylinder remains had a neck fold at the inner edge of the fracture surface. Based upon Figures 1 and 6, a total of three cracks grew subcritically from the sides of the inlet hole. One of these subcritical cracks grew to a critical condition, producing the final rupture; however the two cracks that were diametrically-opposed propagated extensively, while the third crack propagated only to a limited degree. Thus, one of the two diametrically-opposed cracks likely reached critical condition first, leading to a redistribution of stresses in the cylinder and the rapid growth of the remaining two cracks in fast fracture.

The presence, shape, and location of the beach marks on the fracture surface segments (Figures 13 and 14) suggest that the cracks propagated subcritically and slowly for the majority of the flat-faced region, over the 20+ year life of the cylinder. This process continued up to the extent defined by the last beach mark on each side of the inlet hole. This feature is interpreted to mark the onset of rupture by fast fracture. The crack origins for each of the three axial neck cracks were at surface folds on the inside surface below the threads. These postulated origins are consistent with the roughly symmetric morphology of the beach markings. Figure 5 shows cracking from the folds, and Figure 3(b) shows that folds were associated with the main fracture surface. The cracks that developed on the sides of the inlet hole show very similar characteristics and appear to have grown by the same mechanism.

The observed cracks are consistent with the characteristics and morphology of "sustained-load cracking" (SLC) at ambient temperature reported in the literature for similar Al alloys [5, 8-13]. The overall beach marks and implied crack development are consistent with the morphology of cracked regions found at the necks of both US DOT-specification [3, 7] and Australian-specification 6351-T6 aluminum cylinders [6].

Crack Length

To estimate crack length, drawing overlays were developed for the two main neck fracture surfaces, Figures 18 and 19. These overlays correspond to beach marks that

indicate positions of each crack's advancement. In both figures, the blue lines denote visible beach marks in the sub-critical zone, whereas the pink lines denote the extent of the cracking close to the onset of final fast fracture. An interpretation of the blue lines is that they define possible crack arrest (and subsequent re-initiation) positions associated with the internal pressure in the cylinder dropping (through use) to a level at which the local stress intensity, K_I, is below the threshold value necessary for detectable SLC advancement[7].

A measurement was taken from the postulated origin at the folds in the neck to the maximum extent of the pink line for the diametrically-opposed fracture pair. These measurements provide estimates of the crack length at the onset of fast fracture. For the right fracture, this estimate is 47.2 mm; for the left fracture, this estimate is 42.3 mm[8].

Leaking

Fractographic examination of the right-hand fracture surface (1A-2) revealed pathways of SLC propagation to the outer surface of the cylinder. Examples of these pathways are shown with a series of arrows in Figures 16 and 17. The SLC "fingers" reached the outer surface of the cylinder along a line at least 0.25 inches long. Thus, slow progressive crack growth extended to the outer surface of the cylinder in this area, prior to unstable crack growth and rupture. This finding is consistent with the report that the cylinder was leaking prior to rupture. No observations reliably estimate the width of a through-wall crack, or the time such a crack may have been present before rupture of the cylinder occurred. The stability of any such crack (and therefore, the time of leaking) would be expected to depend strongly on the crack shape or aspect ratio[9], the pressure in the cylinder, the temperature, and possibly other factors that cannot be determined from a fractographic study alone.

Examinations of the left-hand fracture surface did not show clear evidence of a similar through-thickness wall penetration.

Time to Rupture

Based on the above arguments, the beach marks outlined by the pink lines on the fracture surfaces (Figures 18 and 19) denote the extent of subcritical SLC propagation. For the mechanism to be operative, the local applied stress intensity, K_I, has to be above the threshold value necessary for detectable SLC advancement. If no significant periods of

[7] Price et al. (1997) show that a threshold stress intensity of about 11 to 13 MPa(m)$^{1/2}$ likely exists based on their analysis of Lewandowski et al.'s data [8] and their observation that no growth has been shown in laboratory tests below 10 MPa(m)$^{1/2}$ [13]. Further simulation work suggests that the threshold stress intensity may be as low as 4 MPa(m)$^{1/2}$ [15]. Threshold behavior is known to occur for other subcritical growth mechanisms such as stress corrosion cracking (SCC); e.g., [14].

[8] The difference in critical crack length on each side is perhaps attributable to local variations in fracture toughness.

[9] Direction-dependent variability in subcritical crack propagation rate can occur with high grain aspect ratios. This direction-dependent variation can lead to high crack aspect ratios.

global arrest are assumed, an estimate of the minimum time to rupture by SLC growth is calculable through the use of average sub-critical SLC growth rates available in the literature (e.g., [8, 12]). To obtain a conservative estimate of the time to rupture, a calculation based on the highest mean propagation rate derived from experimental data [12] is used. This data set is based on specimens with a Pb-level of 100 ppm. Since a higher Pb-level has been shown to result in a higher crack propagation rate [5, 8], the application of 100 ppm Pb data to this cylinder (with a measured Pb-level of < 50 ppm) is conservative with respect to the time for the cracking to develop. An additional degree of conservatism in the crack growth period estimate is realized by disregarding the incubation period from an initial condition with sharp folds at the cylinder neck to the threshold crack-tip K_I condition.

The crack front established on the right fracture by the pink line (Figure 19) results in a crack "length" or extent of 47.2 mm. Using a mean propagation rate [12] of 0.61×10^{-3} mm/hr, the time to rupture is estimated to be 8.8 years. The crack length measured on the left fracture is 42.3 mm, giving an estimated cracking time of 7.9 years using the same propagation rate. Thus, a propagating crack of some size existed at the neck for at least this time frame. This period is a significant portion of the roughly 22 years that the cylinder was in service, following its apparent first hydrostatic test in 1977.

The estimated time-to-rupture is expected to be conservative but must be interpreted in the context of at least two other factors: the cylinder's prior history and possible microstructural influences on the SLC process. With respect to the cylinder history, any exposure to elevated temperature would increase the crack propagation rate, as would any moderate or severe overpressurization, if done. In addition, whenever the cylinder was operating at reduced pressures, the crack propagation would be slower or possibly arrested. Secondly, microstructural influences would include local variations in grain size, grain aspect ratio and texture, and these may have an effect on crack growth rate that is not captured in the experimental data set used in the estimate. Both of these factors are expected to influence the time to rupture.

8.0 Summary and Conclusions

A metallurgical examination of the remains of a US-DOT-E6498-2216 type aluminum gas cylinder manufactured by Luxfer USA showed the following results.

- This 1977-vintage cylinder meets the chemical and mechanical property requirements of both the DOT E6498 and current US-DOT-3AL specifications in 49 CFR 178.46 for AA6351-T6 alloy, including lead (Pb) and bismuth (Bi) levels.

- Small cracks were found originating at folds on the interior wall in the neck region near the inlet hole. These folds existed at the time of the cylinder's manufacture.

- The cylinder failed when one of two diametrically-opposed sub-critical cracks in the neck region grew to critical size. The initial cracking appears to have developed from folds at the inside surface of the neck region.

- The apparent origin location and overall appearance of the fracture is consistent with sustained-load cracks (SLC) reported in the literature for similar Al alloys. The crack size at the time of rupture appears to be defined by the macroscopic beach marks that were farthest away from the inlet hole on the flat-faced (i.e., radial) portions of the fracture surfaces.

- Fractography established an SLC crack path through the wall to the outside surface, consistent with reports that the cylinder was leaking prior to rupture.

- An estimate of the time-to-rupture based on measurements of the crack lengths and on published crack-growth rate data indicates that a crack of some size existed in the neck region for at least 8 years prior to rupture.

9.0 References

1. J. E. Hatch, Ed., (1984). Aluminum: Properties and Physical Metallurgy, American Society for Metals, Metals Park, OH, p. 363.
2. "Standard Hardness Conversion Tables for Metals," Standard E 140-97, American Society for Testing and Materials, West Conshohocken, PA, 1999.
3. "Metallurgical Evaluation of a DOT-E6498-2216 Cylinder", Failure Analysis Associates, Inc. Technical Report to RSPA, U.S. Department of Transportation, January 1997.
4. J. H. Smith (1987). "Evaluation of Cracking in Aluminum Cylinders", NBSIR 86-3492, Institute for Materials Science and Engineering, National Bureau of Standards (NBS), U.S. Dept. of Commerce, Gaithersburg, MD.
5. M. Guttmann, B. Quantin, and Ph. Dumoulin (1983). "Intergranular creep embrittlement by non-soluble impurity: Pb precipitation hardened Al-Mg-Si alloys", Metal Sci., Vol. 17, No. 3, pp. 123-140.
6. J. W. H. Price, R. N. Ibrahim and D. Ischenko (1996). "Cracking in Aluminum 6061 and 6351 Gas Cylinders", Proc. Int. Conf. on Pressure Vessel Technology, Vol 1., American Society of Mechanical Engineers (ASME), Montreal, Canada, pp. 337-343.
7. Cylinder neck fragment examined by FaAA from the National Institute of Science and Technology (NIST). Per. com., J. H. Smith (1996), Materials Science and Engineering Laboratory, NIST, U.S. Dept. of Commerce, Gaithersburg, MD.
8. J. J. Lewandowski, Y. S. Kim, and N. J. H. Holroyd (1992). "Lead-Induced Solid Metal Embrittlement of an Excess Silicon Al-Mg-Si Alloy at Temperatures of -4°C to 80° C", *Met. Trans. A.*, Vol. 23A, pp. 1679-1689.
9. Y. S. Kim, N. J. H. Holroyd, and J. J. Lewandowski (1989). "Pb-Induced Solid-Metal Embrittlement of Al-Mg-Si Alloy at Ambient Temperatures", *Proc. Environment-Induced Cracking of Metals*, National Association of Corrosion Engineers (NACE), pp. 371-377.
10. J. J. Lewandowski, V. Kohler, and N. J. H. Holroyd (1987). "Effects of Lead on the Sustained-load Cracking of Al-Mg-Si Alloys at Ambient Temperatures", *Mat. Sci & Eng.*, Vol. 96, pp. 185-195.
11. H. L. Stark and R. N. Ibrahim (1992). "Crack Propagation in Aluminum Gas Cylinder Neck Material at Constant Load and Room Temperature", Eng. Fracture Mechanics, Vol. 41, No. 4, pp. 569-575.
12. H. L. Stark and R. N. Ibrahim (1988). "Crack Propagation at Constant Load and Room Temperature in an Extruded Aluminum", Eng. Fracture Mechanics, Vol. 30, No. 3, pp. 409-414.
13. J. W. H. Price, R. N. Ibrahim and D. Ischenko (1997). "Sustained Load Crack Growth Leading to Failure in Aluminum Gas Cylinders in Traffic", Engineering Failure Analysis, Vol. 4, No. 4, pp. 259-270.
14. J. M. Barsom and S. T. Rolfe (1987). Fracture and Fatigue Control in Structures, 2nd. Ed., Prentice-Hall, Inc., Englewood Cliffs, NJ, p. 347.
15. P. M. Singh, N.J.H. Holroyd, J. J. Lewandowski and J. T. Evans (1992). "Monte-Carlo Simulation of Lead Induced Slow Crack Growth in Al-Mg-Si Alloys", Parkins Symposium on Fundamental Aspects of Stress Corrosion Cracking, Edited by S. M. Bruemmer, E.I. Meletia, R. H. Jones, W.W. Gerberich, F. P. Ford and R.W. Stanchle, The Minerals Metals & Materials Society (TMS), pp. 567-583.

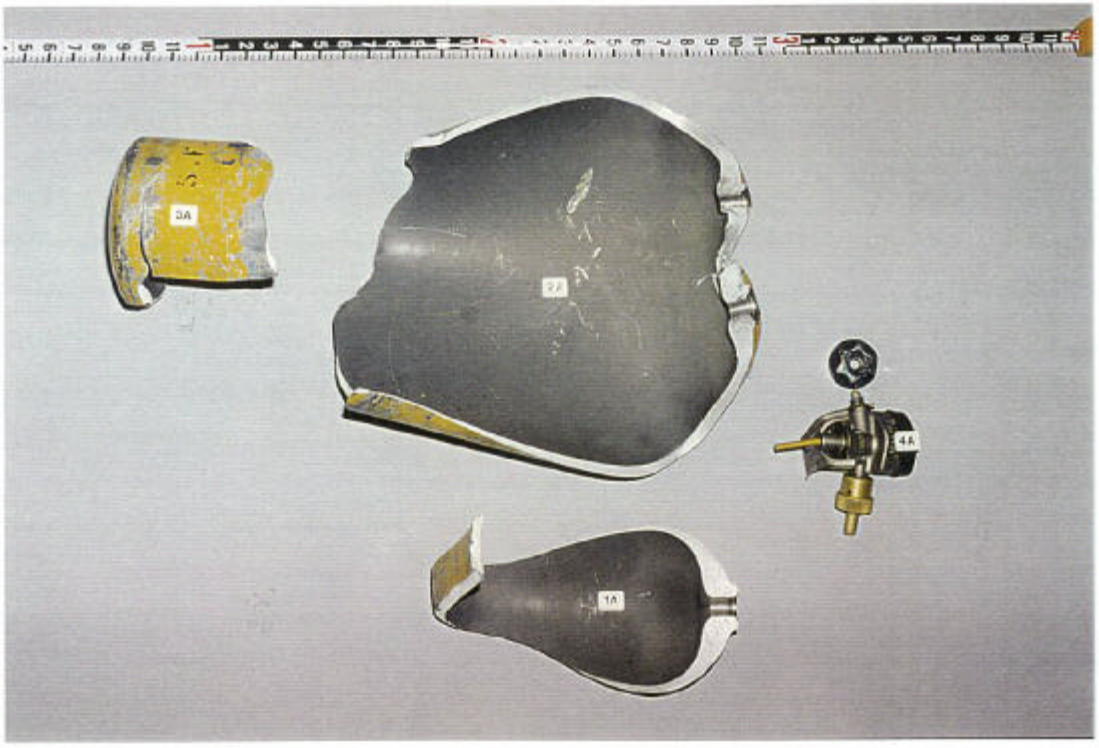

(a)

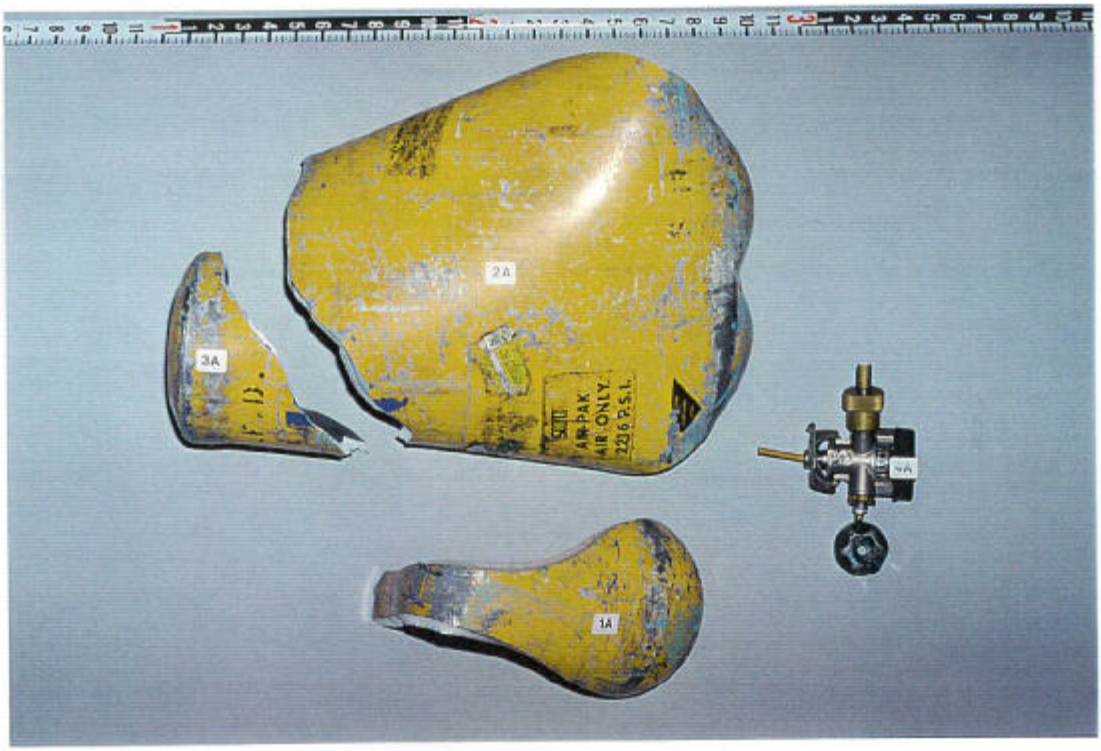

(b)

Figure 1: **Gas cylinder fragments in their as-received condition.**
(a) Inside surface and fracture surfaces (Photo ID: DC18234-R1E11)
(b) Outside surface (Photo ID: DC18234-R1E9)

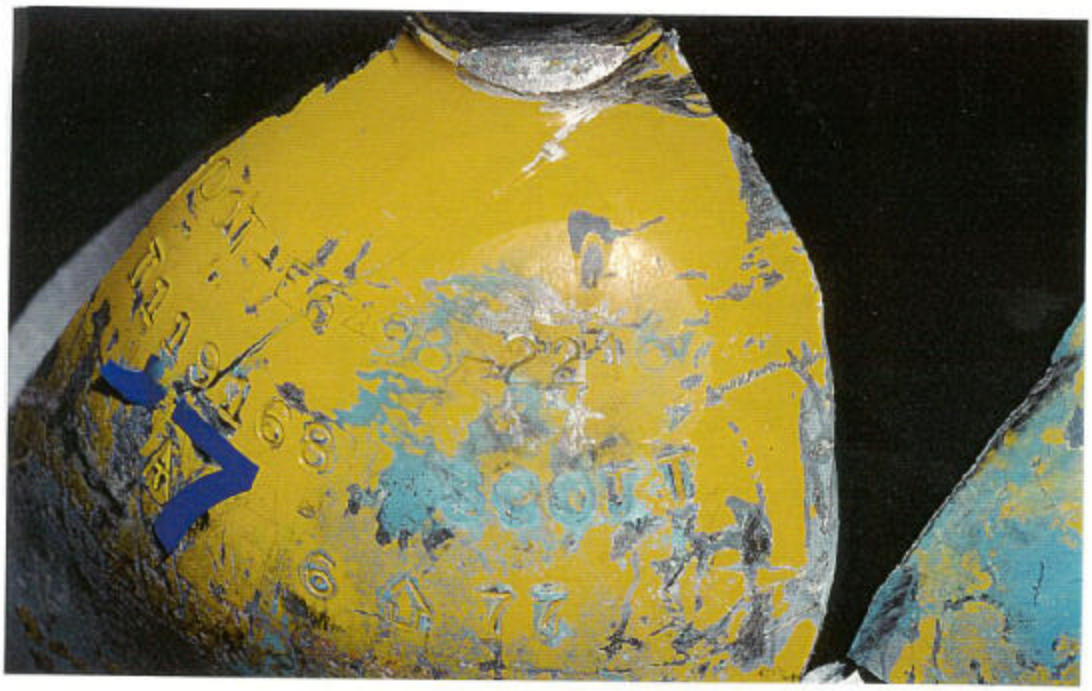

(a)

(b)

Figure 2: **Neck Stampings**
(a) Exemption, serial number and first hydrostatic test.
(Photo ID: DC18234-R2E3)
(b) Inspection markings
(Photo ID: DC18234-R2E5)

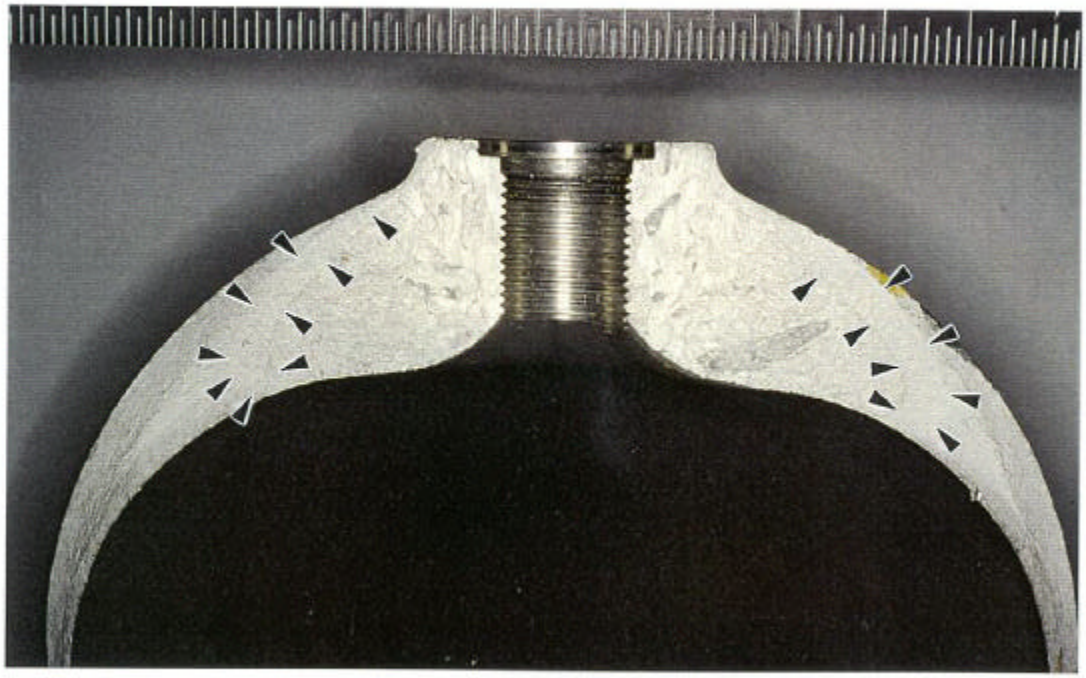

(a)

(b)

Figure 3: **Detail of the fracture surface at the cylinder neck.**
(a) Fracture surface at cylinder neck (Photo ID: DC18234-R2E29)
(b) Detail of fracture surface at the neck. (Photo ID: DC18234-R2E6)
Note the beachmarks shown at the arrows.

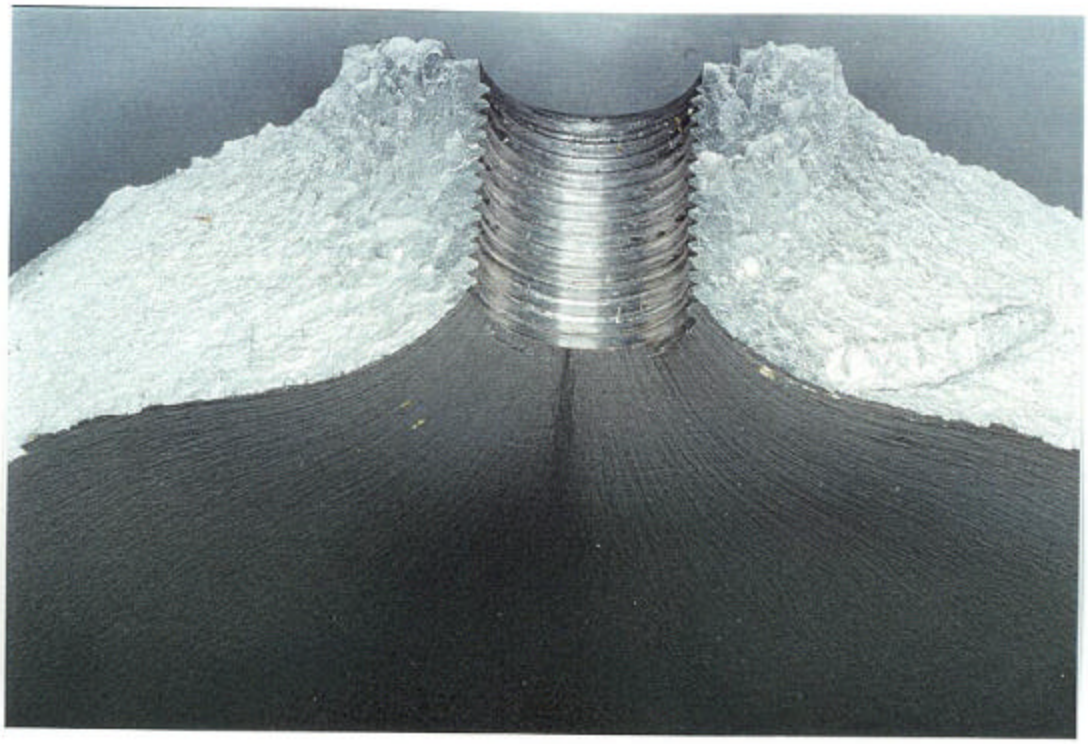

Figure 4: **Folds or cusps at the cylinder neck.**
Note axial and circumferential orientations of the folds on the inner wall of the cylinder.

(Photo ID: DC18234-R4E15)

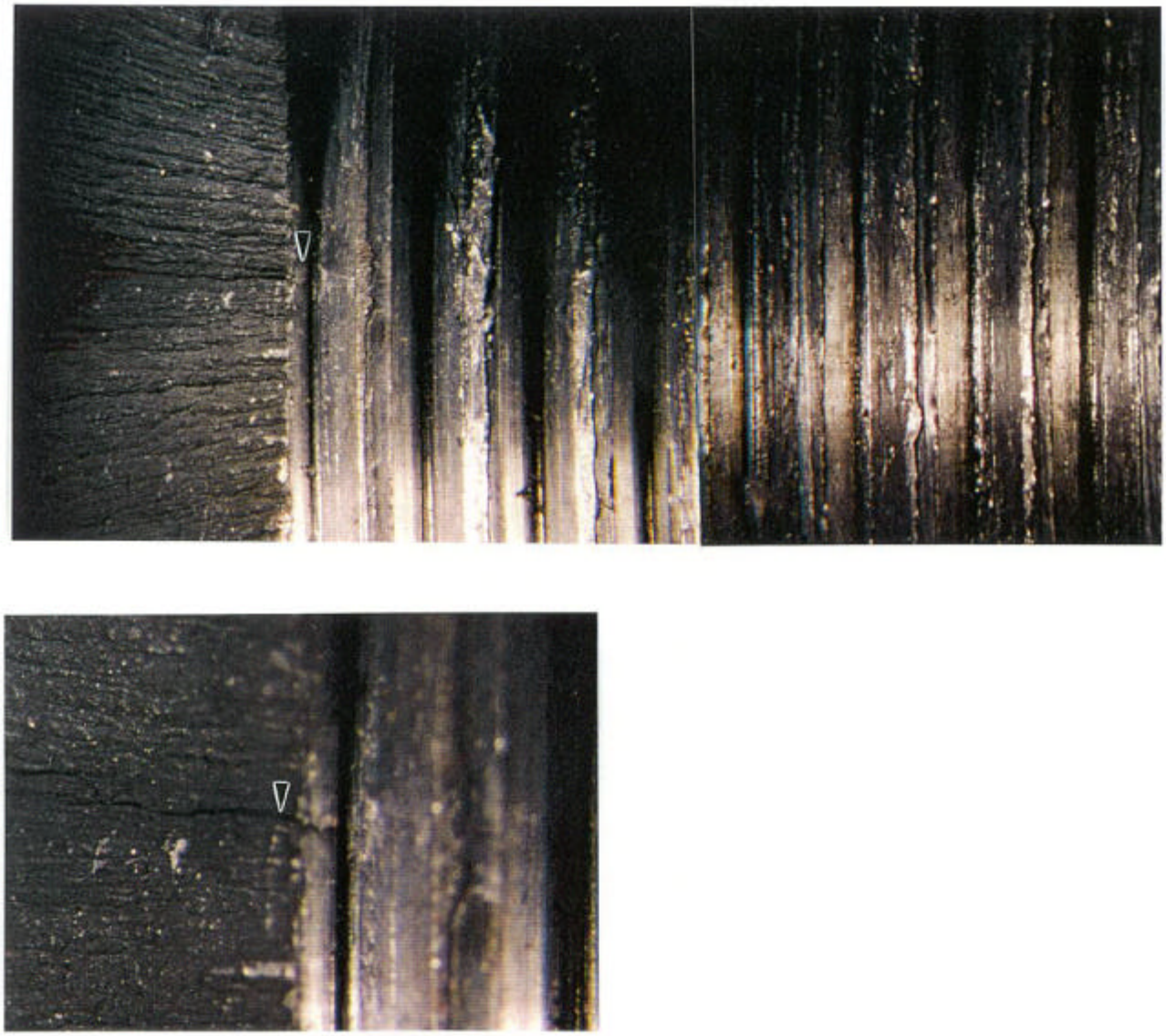

Figure 5: **Crack from a neck fold, extending across the lowest thread.** (Photo IDs: DC18234-R5E7, -R5E12, -R5-E15)
Note the crack shown at the arrows.

Figure 6: **Sectioning of cylinder fragment 2A to remove mechanical test specimens.**

(Photo ID: DC18234-R6E11)

Figure 7: **Sectioning of the cylinder neck region.**
Specimens 1A-1 and 1A-2 were cut from the neck for fractography. Specimen 1A-3 was cut behind 1A-2 for hardness testing and metallography.

(Photo ID: DC18234-R3E15)

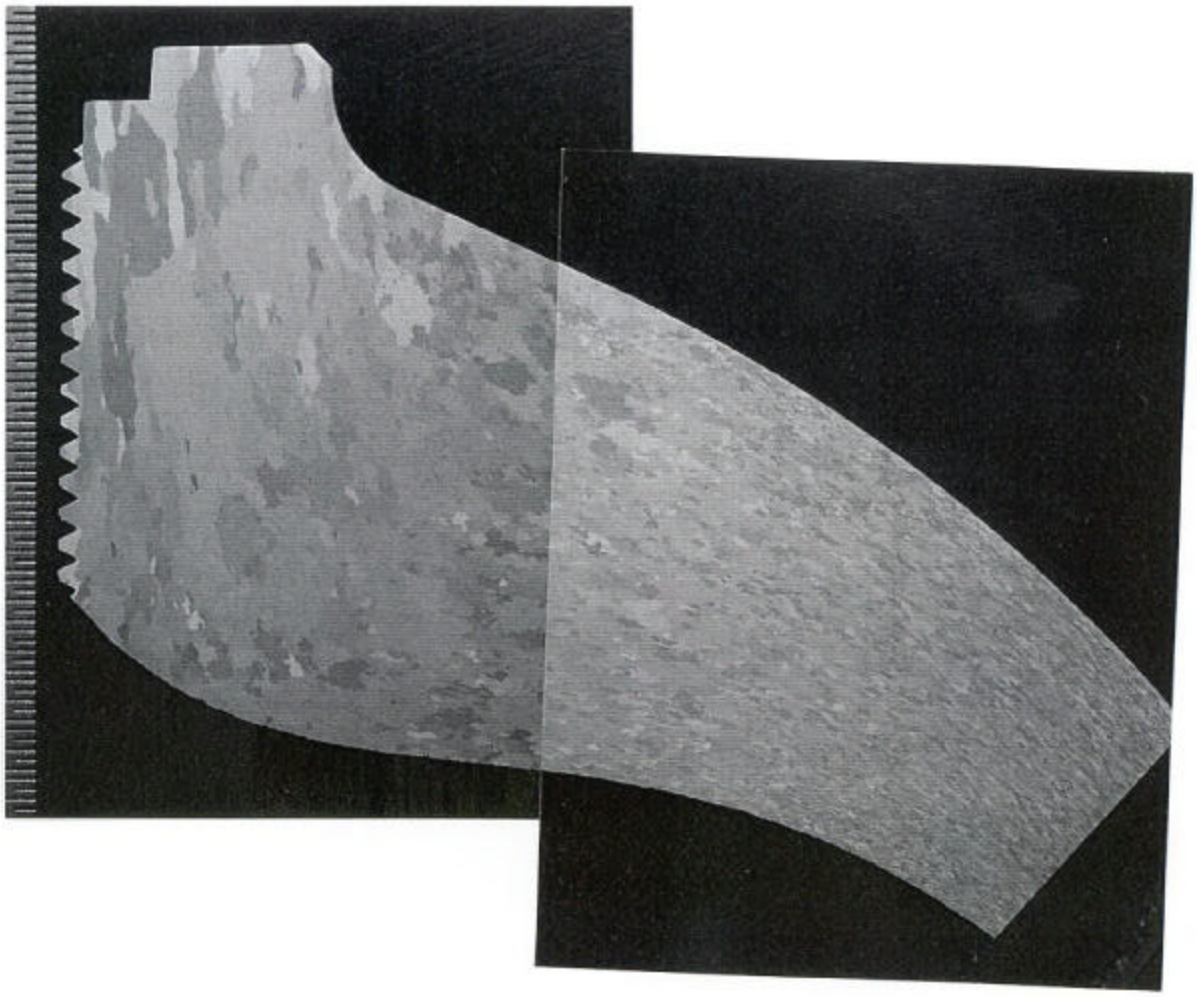

Figure 8: **Metallographic section of the cylinder neck, specimen 1A-3.** From the thick section near the threads toward the cylinder sidewall, there is significant reduction in grain size and an increase in grain aspect ratio. The grains are oriented in the forming direction of the cylinder.

Magnification: 2.7x
Etchant: 1% HF (aq)
(Photo ID: DC18234-PAL-11,-12-7/12/99)

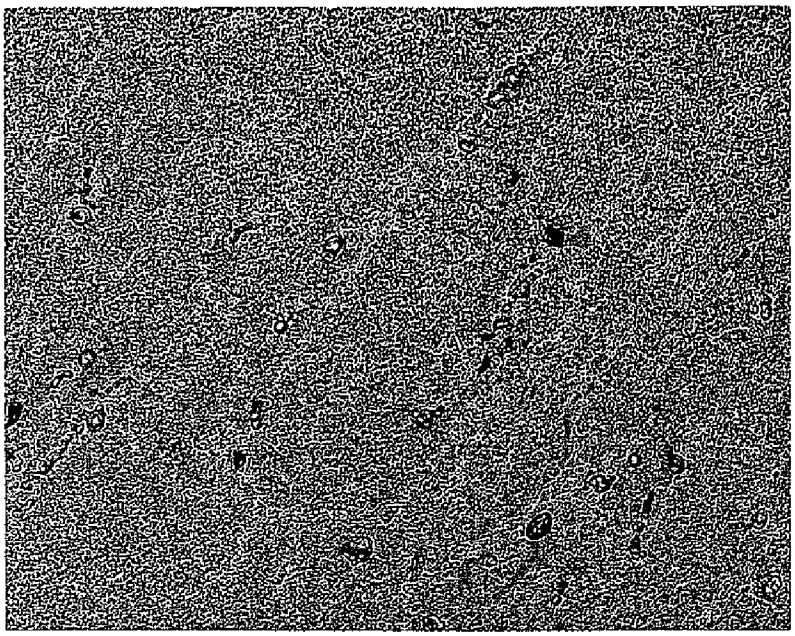

Figure 9: **Microstructure near cylinder neck, 500x.**
The structure is typical of AA6351 in the T6 condition.

Etchant: 1% HF (aq)
(Photo ID: DC18234-PAL-17-6/30/99)

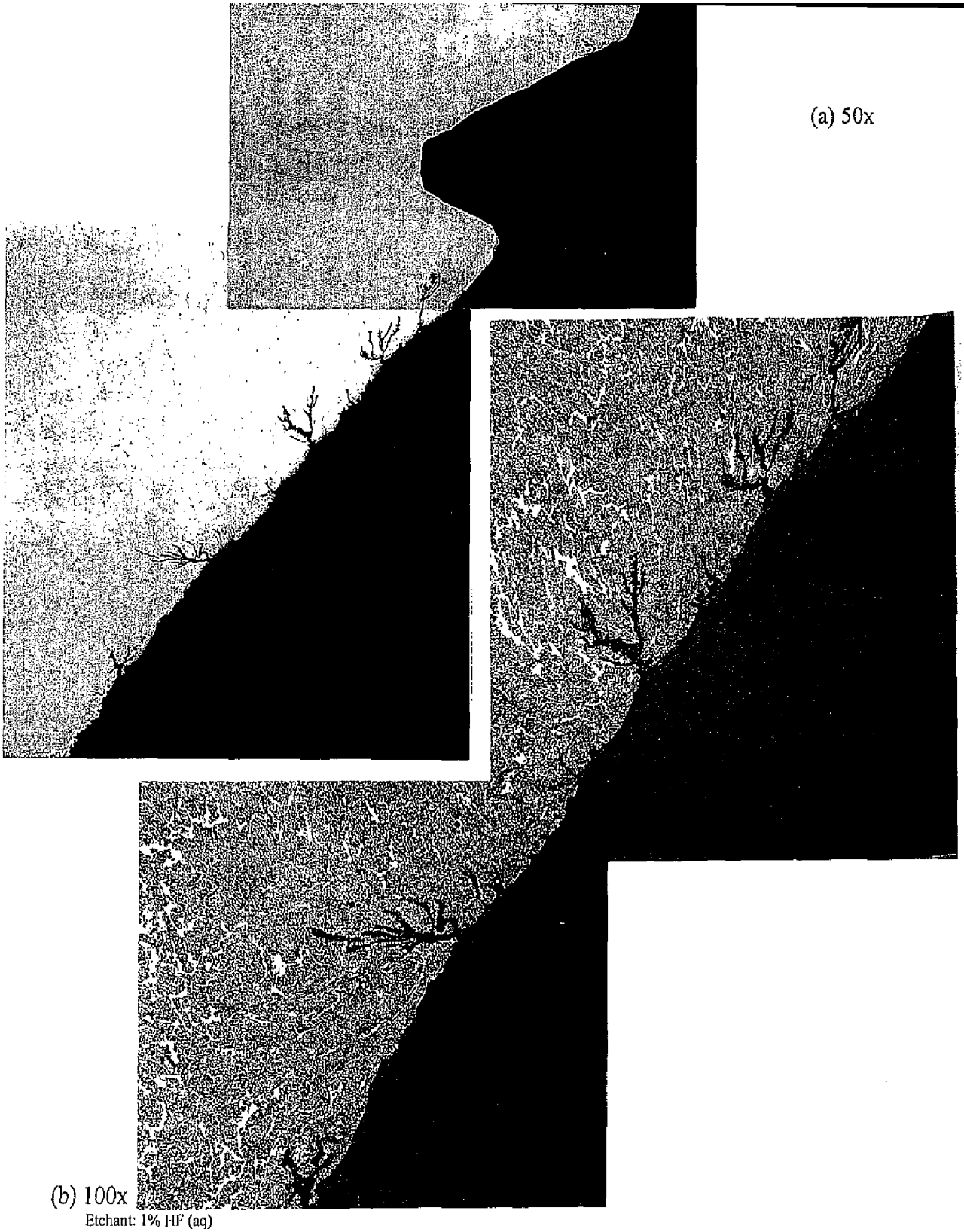

Figure 10: Branching cracks at the inside of the cylinder wall.

Photo IDs: (a) DC18234-PAL-3,-4-6/25/99
(b) DC18234-PAL-9-10-6/30/99

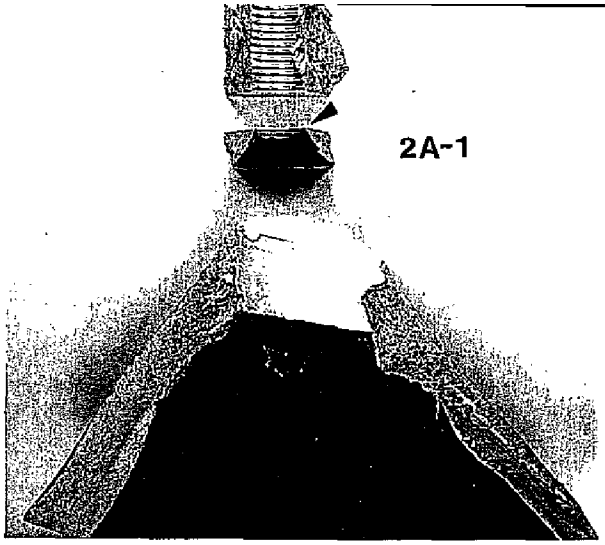

(a)

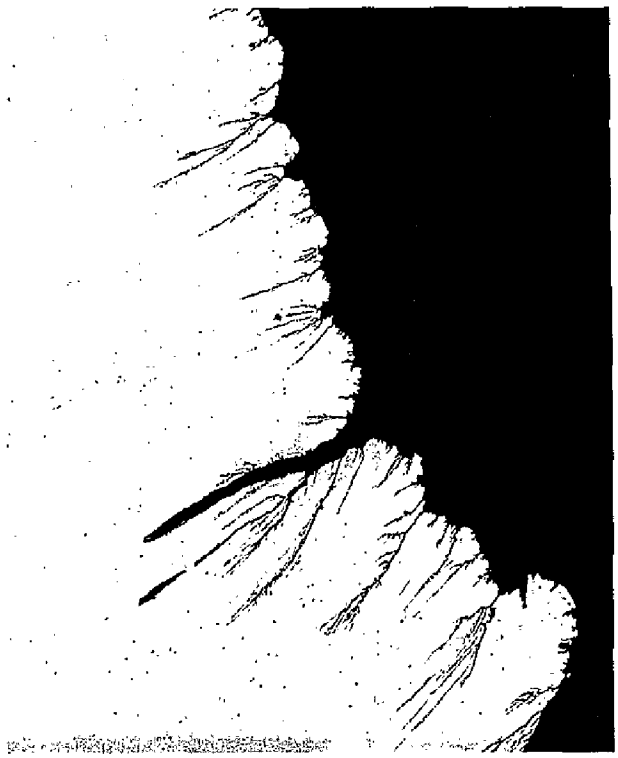

(b) (c)

Figure 11: Metallographic section at the base of the neck threads.
(a) The arrow indicates the plane of polish.
(Photo ID: DC18234-PAL-1-8/9/99)
(b) (c) Branching cracks extend from the base of the threaded region into the cylinder neck.
Magnification: (b) 50x, (c) 100x
Etchant: 1% HF (aq)
(Photo IDs: DC18234-PAL-3,-4-8/9/99)

Figure 12: Cracking parallel to a flat-faced fracture surface at the neck, 100x.

Etchant: 1% HF (aq)
(Photo ID: DC18234-PAL-11,-12-8/9/99)

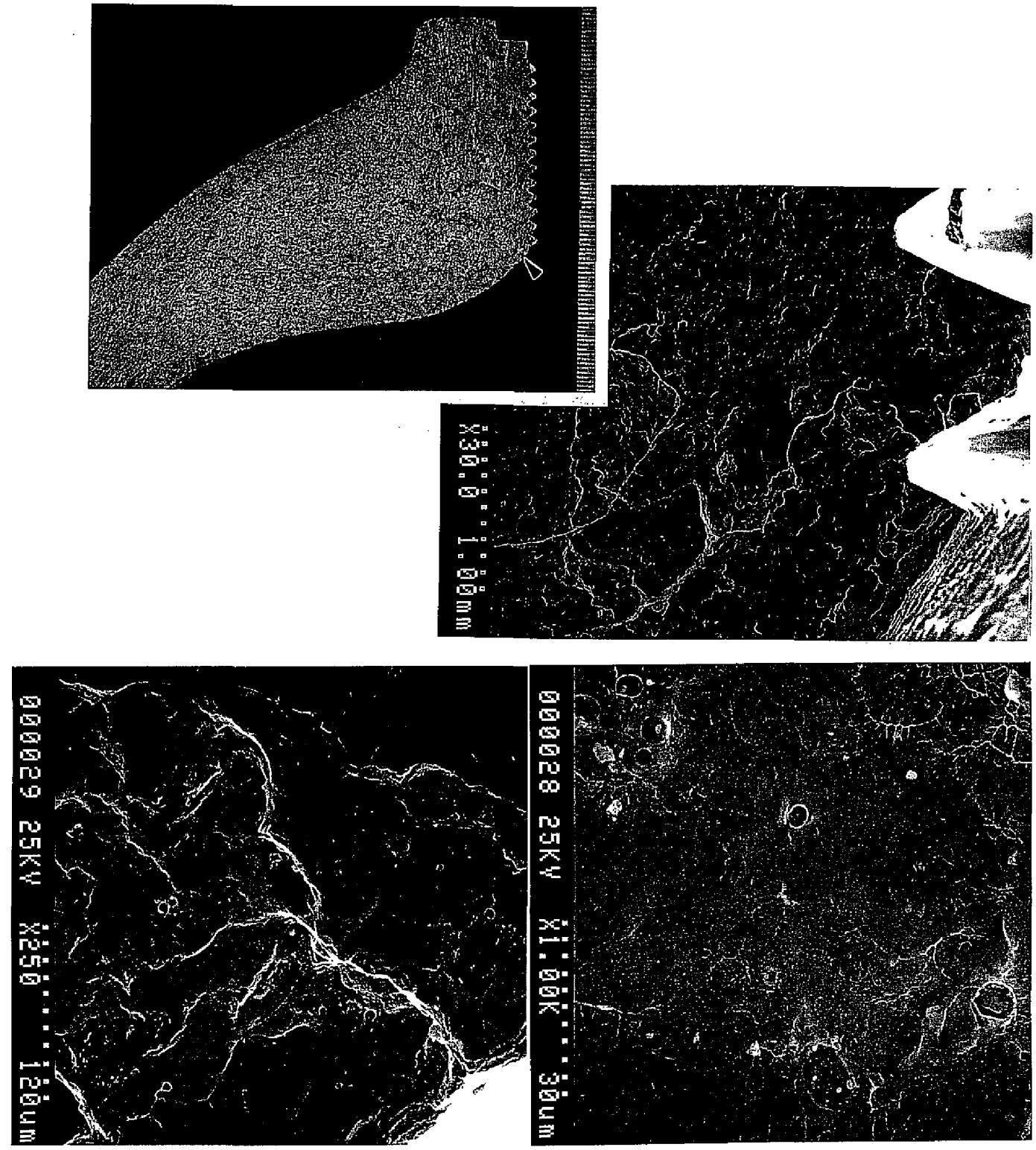

Figure 13: SEM fractography of specimen 1A-1, near fracture origin.

Photo IDs: (a) DC18234-PAL-1-6/25/99 (b) DC18234-CEM-3-7/8/99
(c) DC18234-CEM-2-7/8/99 (d) DC18234-CEM-1-7/8/99

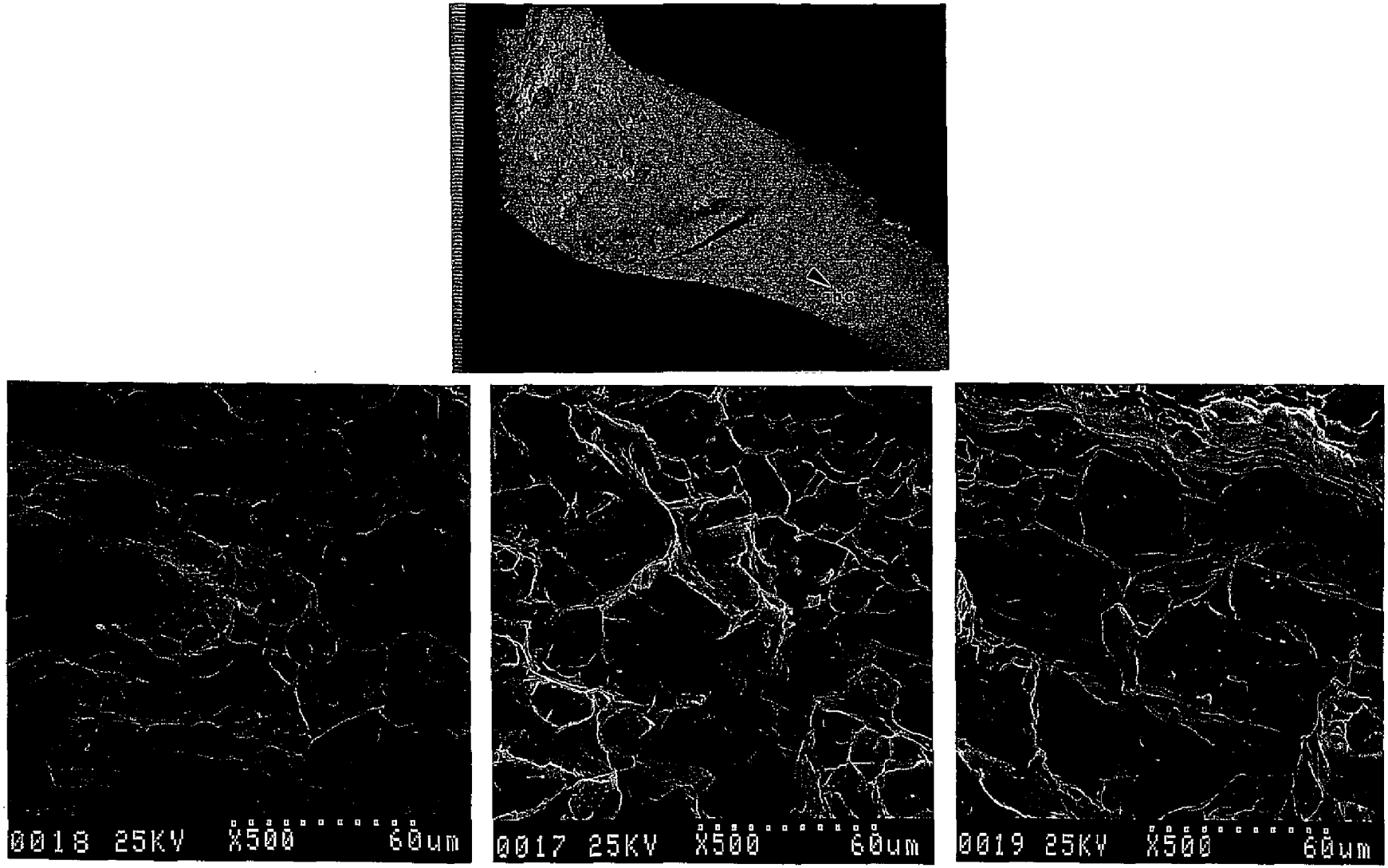

(a) (b) (c)

Figure 14: SEM fractography of specimen 1A-2, at first beachmark.

(Photo IDs: DC18234-PAL-2-6/25/99, -PAL-18,-17,-19-7/7/99))

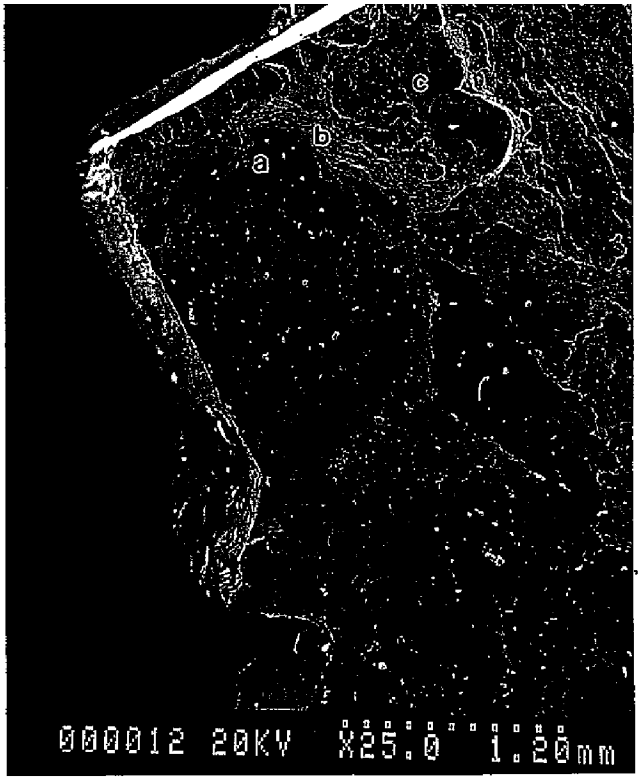

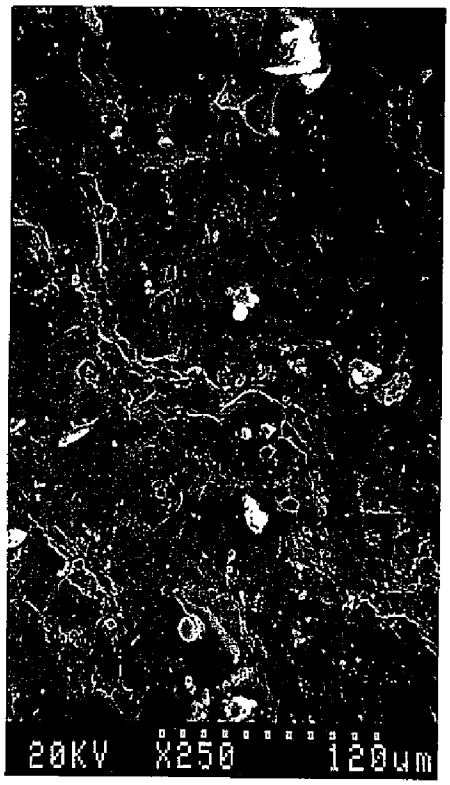

(a)

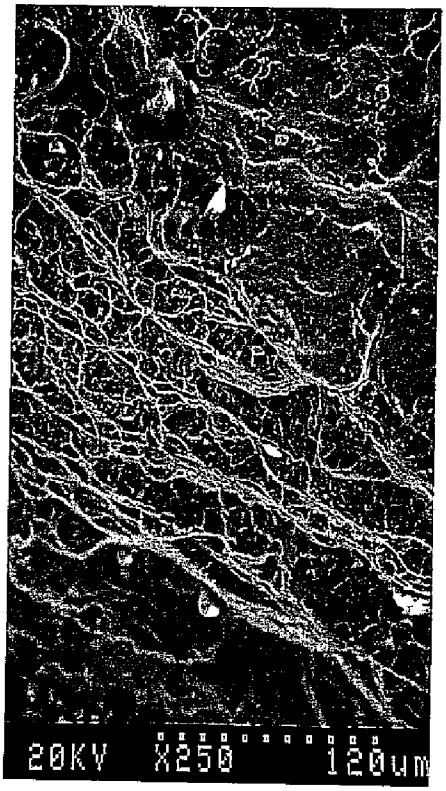

(b)

(c)

Figure 15: SEM fractography of specimen 1A-2, at top of neck.

(Photo IDs: DC18234-CEM-9,-10,-12,-14-6/29/99)

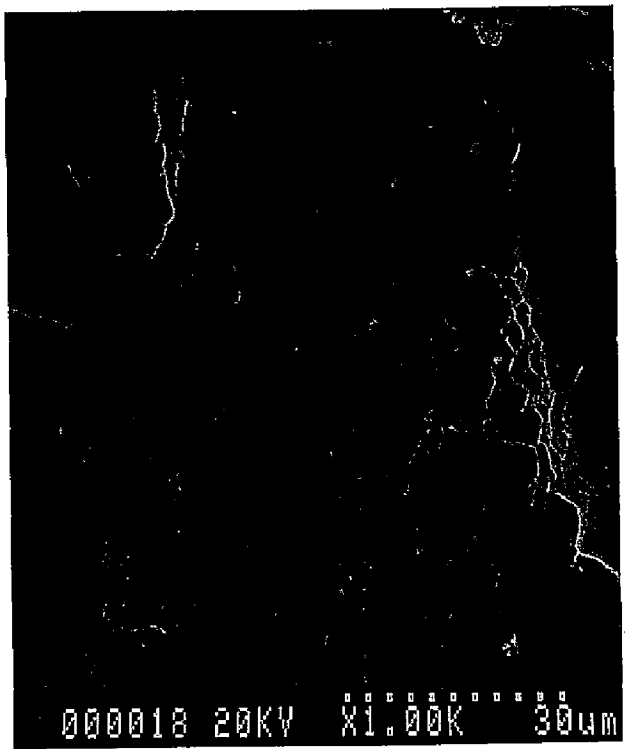

Figure 15: **SEM fractography of specimen 1A-2, at top of neck (continued).** Detail of Figure 15(c).

(Photo ID: DC18234-CEM-15-6/29/99)

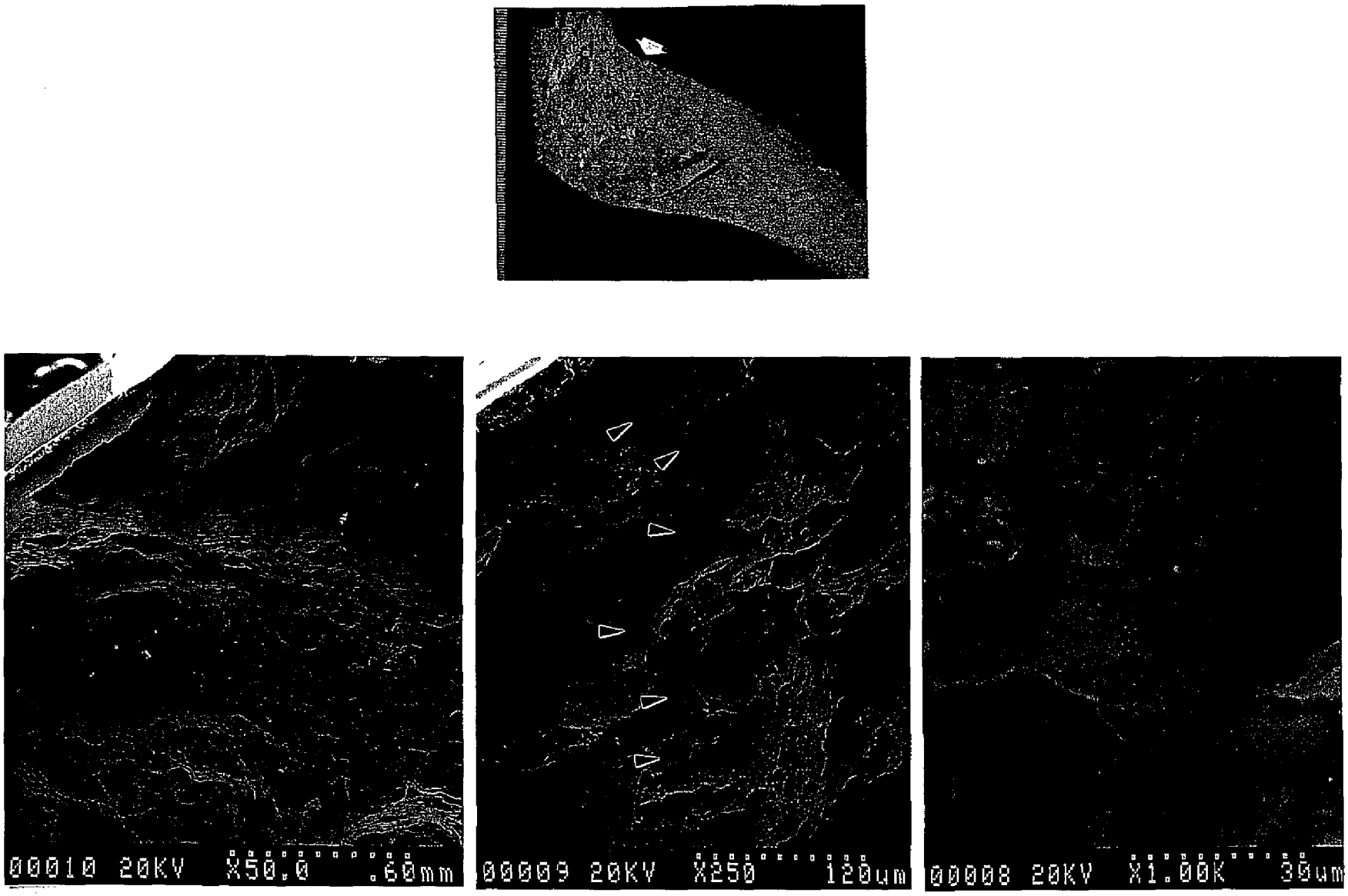

Figure 16: **SEM fractography of specimen 1A-2, at outer surface.**

(Photo IDs: DC18234-PAL-2-6/25/99, -CEM-10,-9,-8-8/18/99)

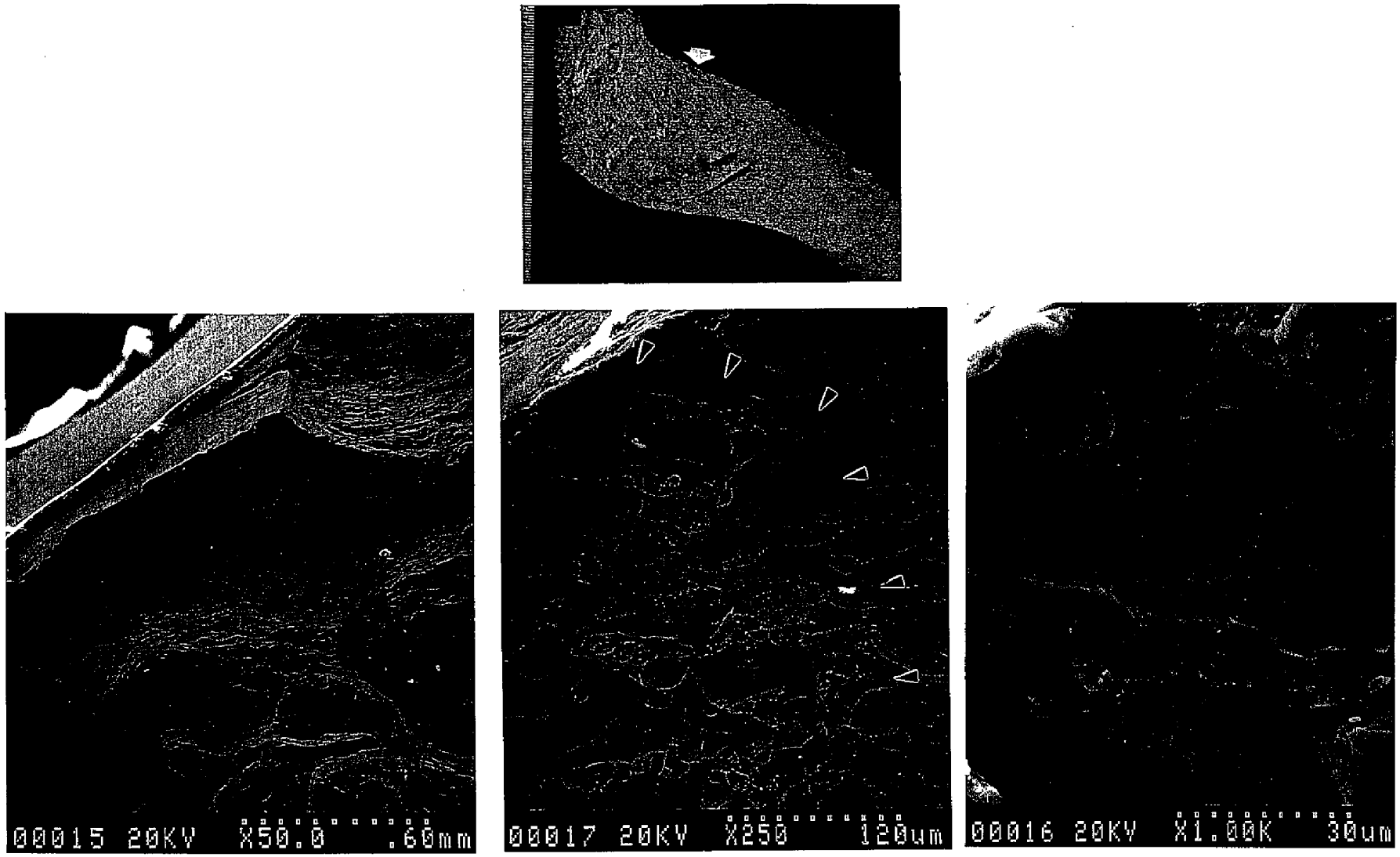

Figure 17: **SEM fractography of specimen 1A-2, at outer surface.**

(Photo IDs: DC18234-PAL-2-6/25/99, -CEM-15,-17,-16-8/18/99)

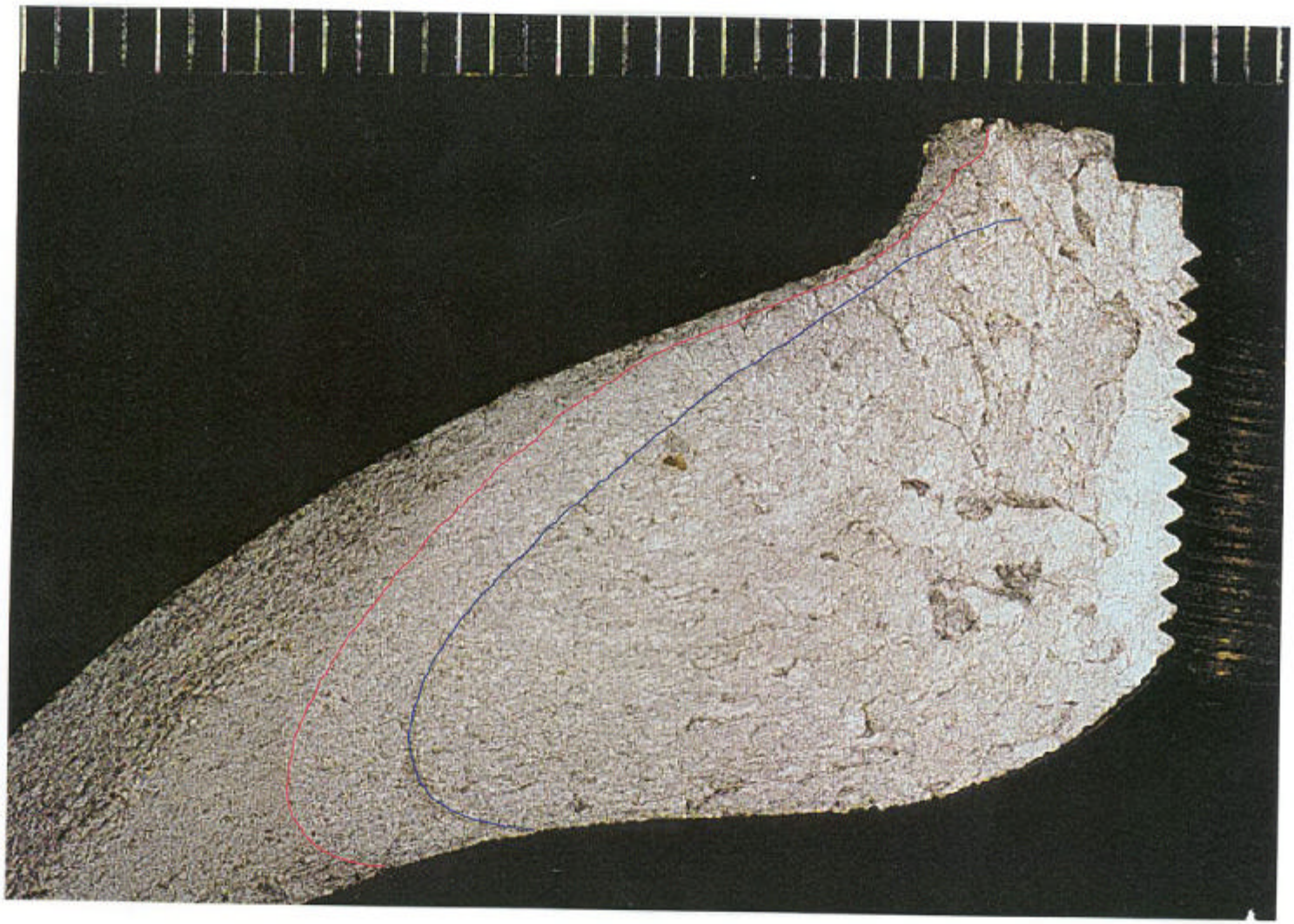

Figure 18: **Fracture surface 1A-1, showing crack fronts at different time points (beach marks).**

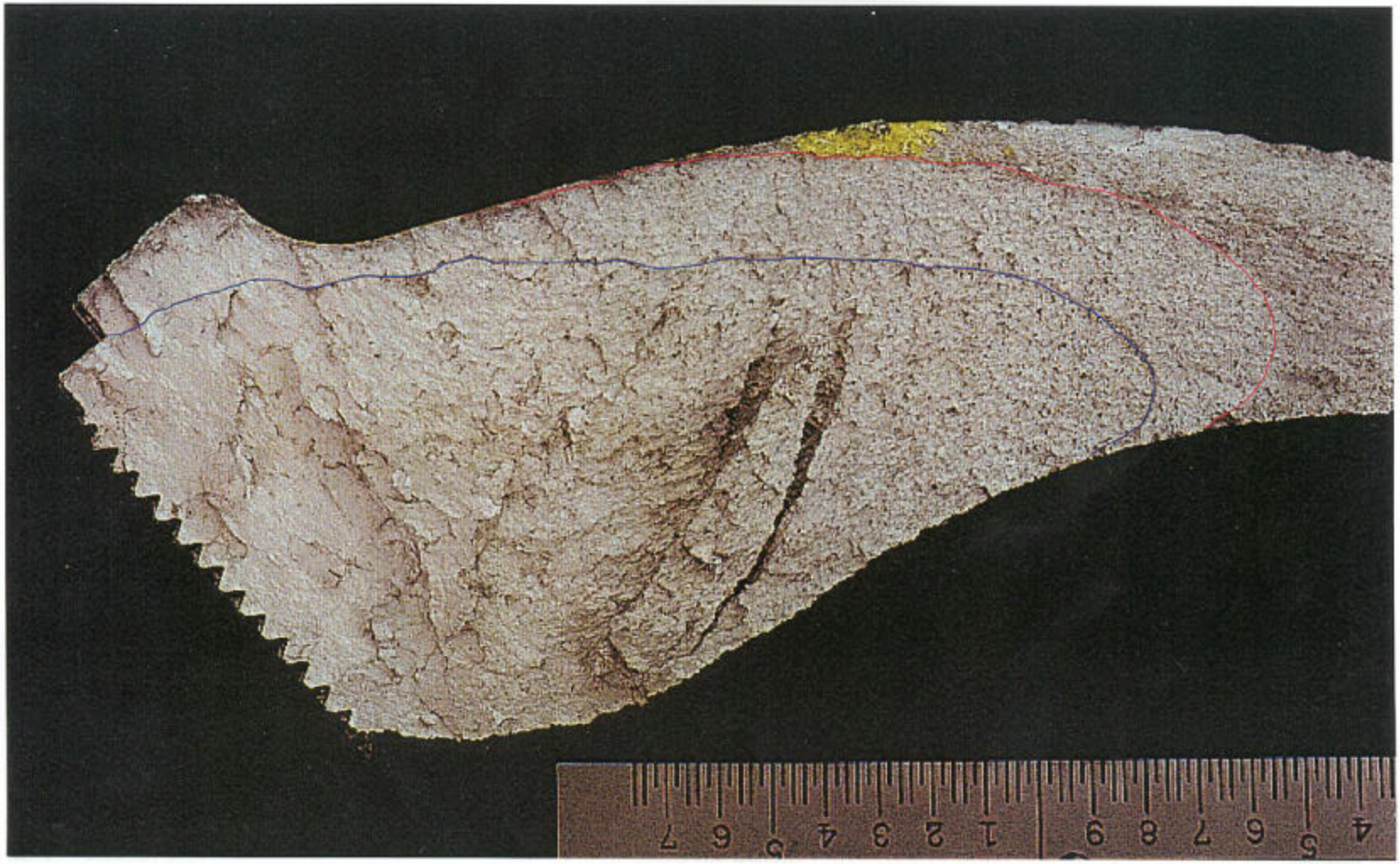

Figure 19: **Fracture surface 1A-2, showing crack fronts at different time points (beach marks).**

Appendix A: Detailed Photodocumentation of Cylinder

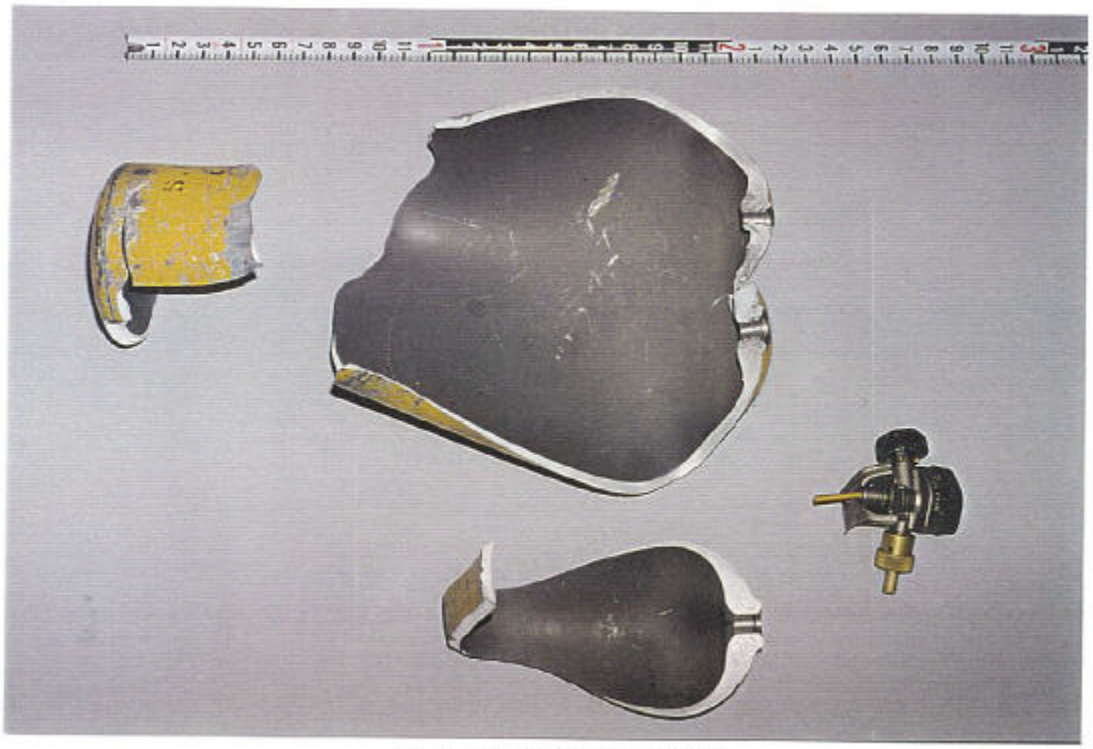

Photo ID: DC18234-R1E5

Photo ID: DC18234-R1E6

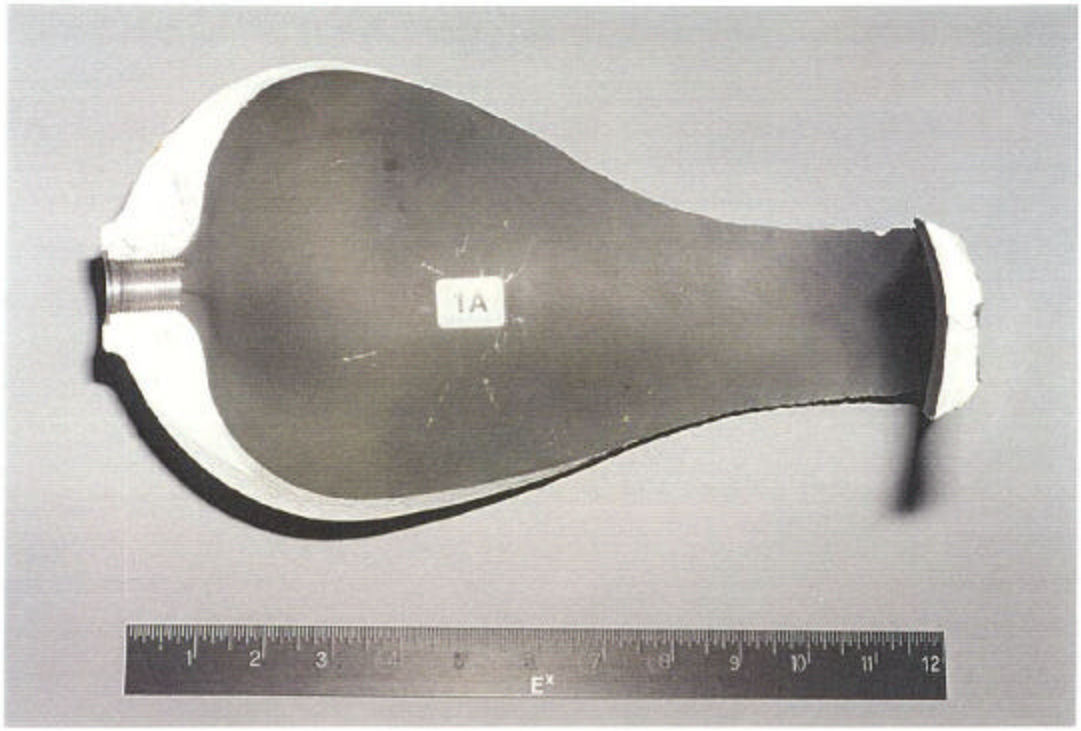

Photo ID: DC18234-R1E14

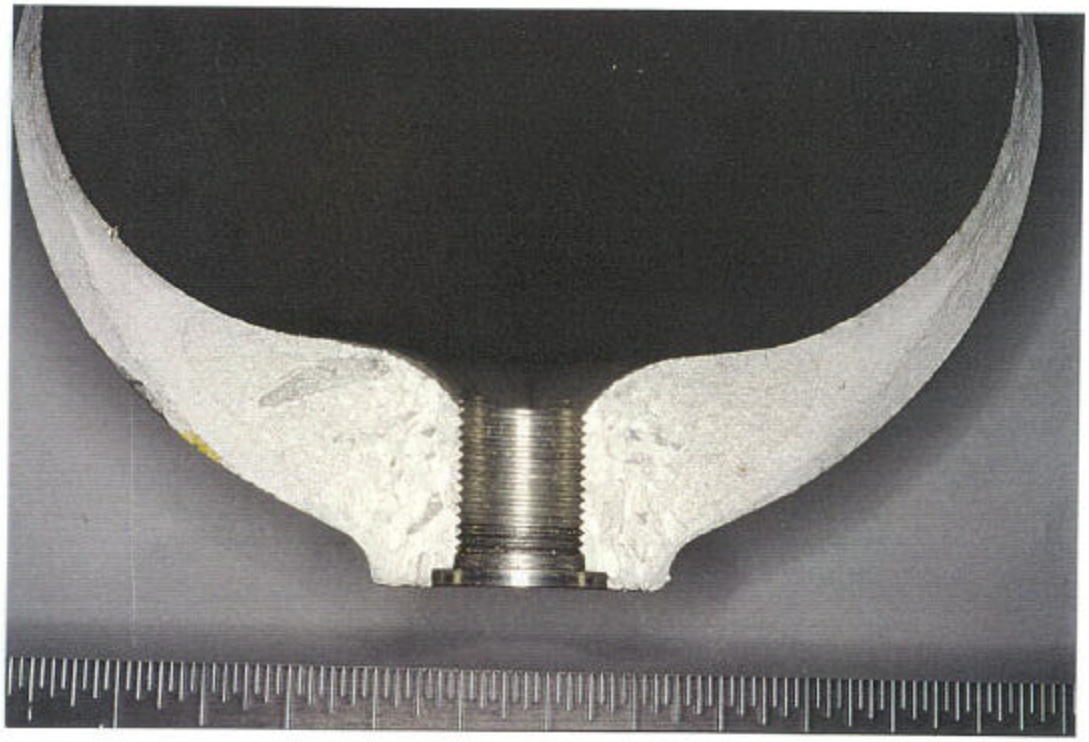

Photo ID: DC18234-RE29

Photo ID: DC18234-R1E15

Photo ID: DC18234-R1E16

Photo ID: DC18234-R1E17

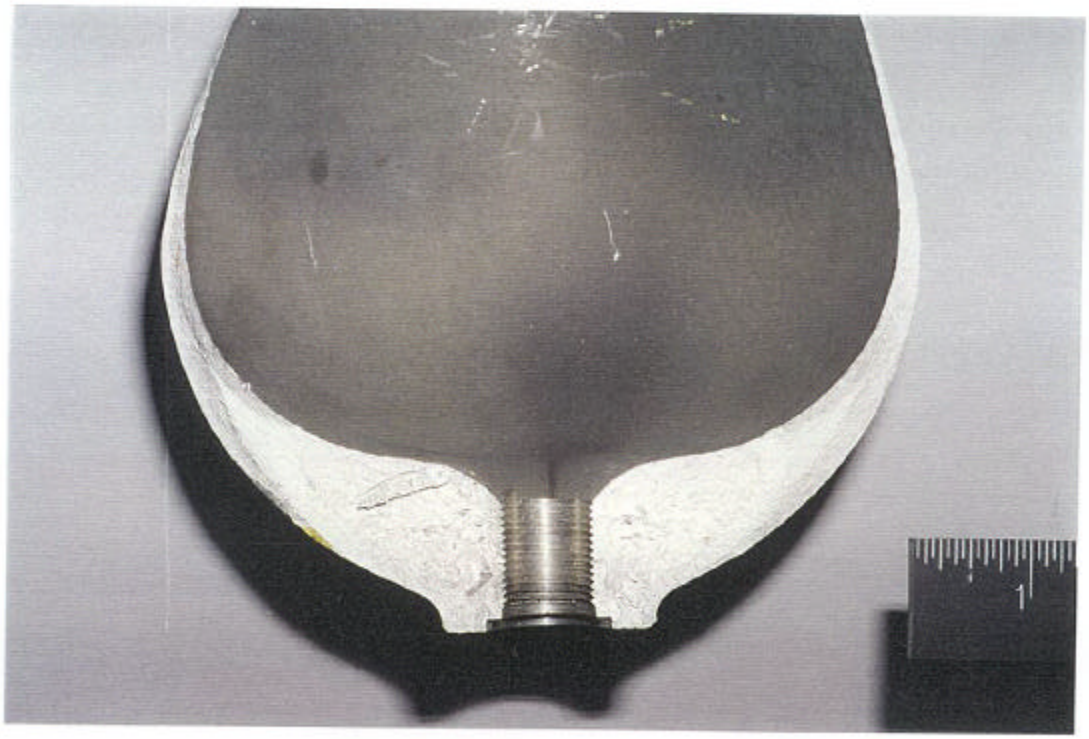

Photo ID: DC18234-R1E18

Photo ID: DC18234-R1E21

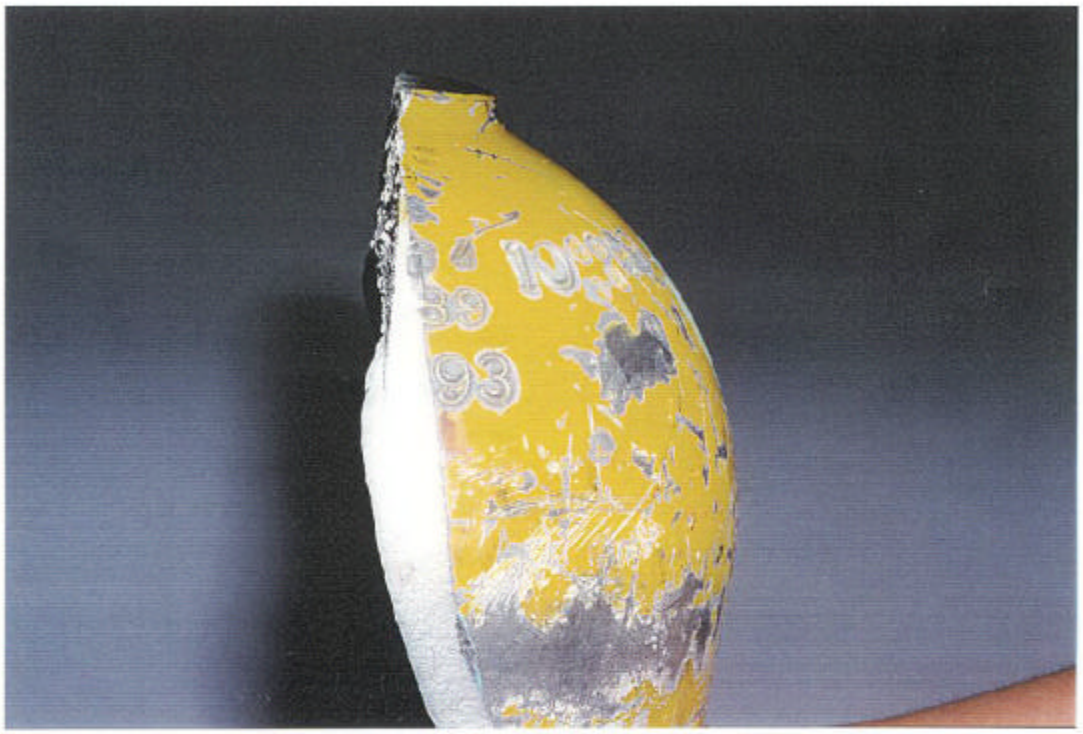

Photo ID: DC18234-R1E22

Photo ID: DC18234-R1E24

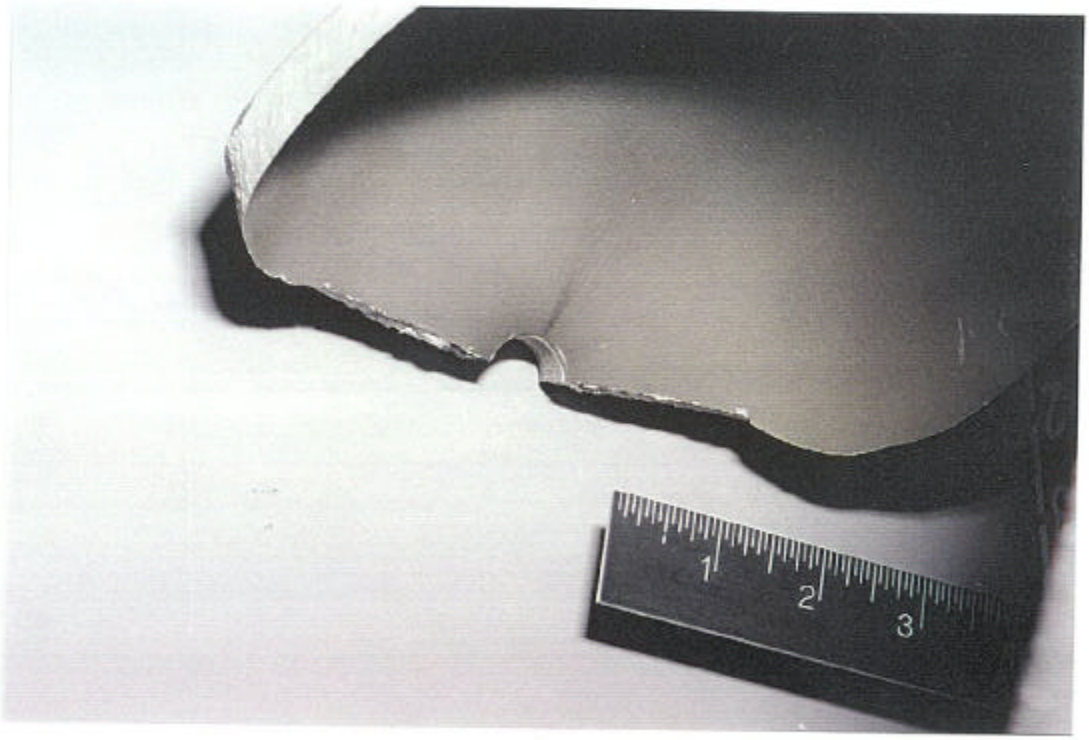

Photo ID: DC18234-R1E25

Photo ID: DC18234-R1E26

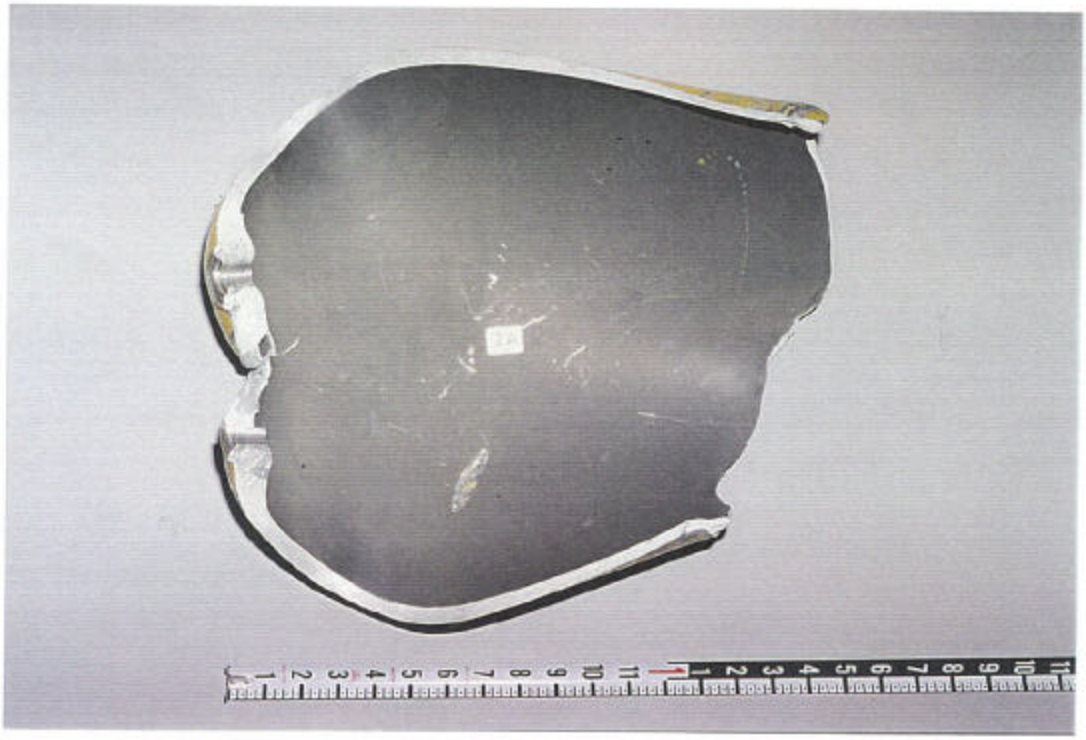

Photo ID: DC18234-R1E28

Photo ID: DC18234-R1E30

Photo ID: DC18234-R1E32

Photo ID: DC18234-R1E33

Photo ID: DC18234-R1E34

Photo ID: DC18234-R1E35

Photo ID: DC18234-R1E36

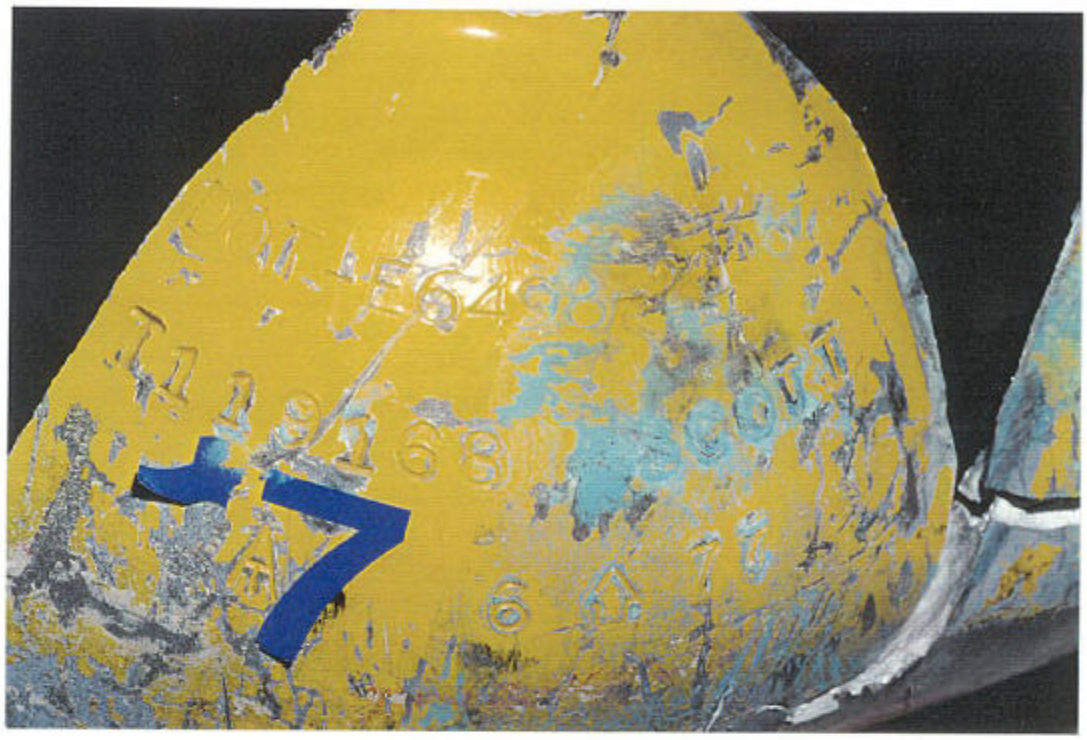

Photo ID: DC18234-R1E37

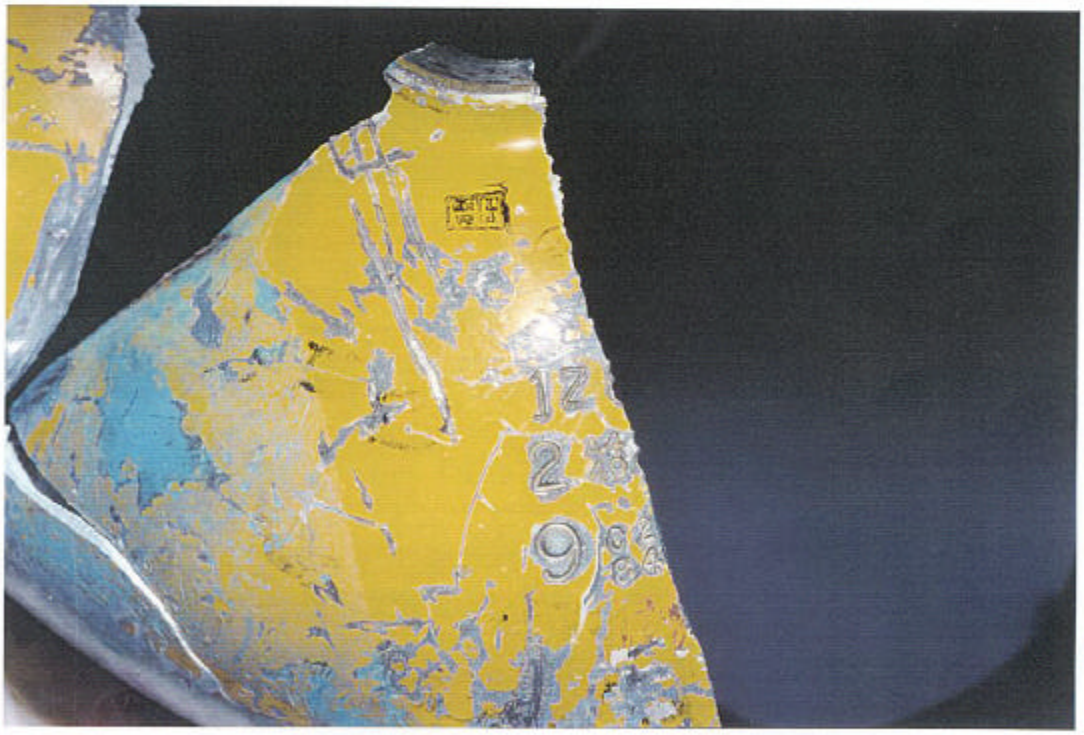

Photo ID: DC18234-R2E4

Photo ID: DC18234-R2E5

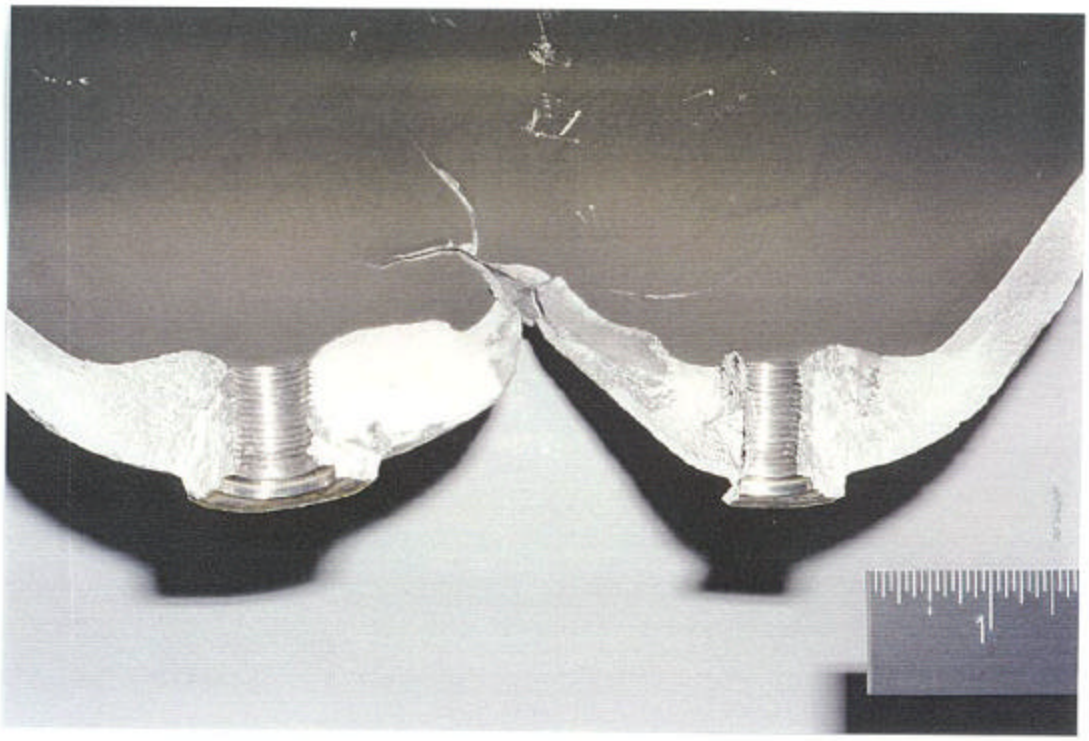

Photo ID: DC18234-R2E8

Photo ID: DC18234-R2E9

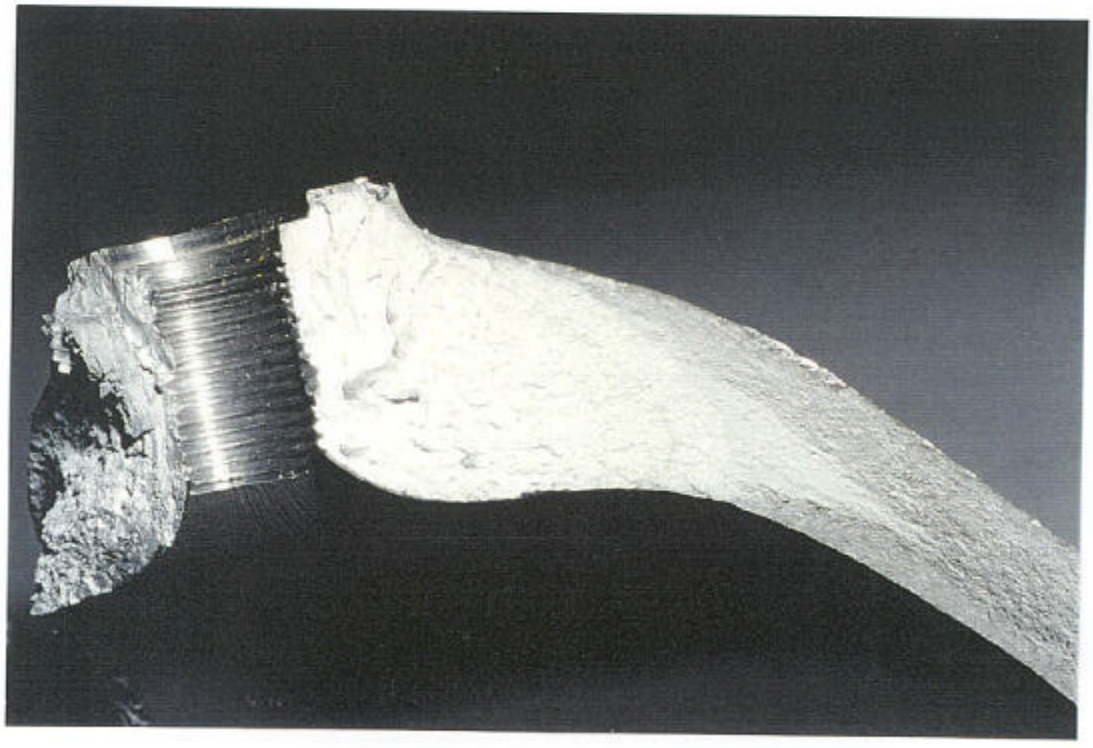

Photo ID: DC18234-R2E10

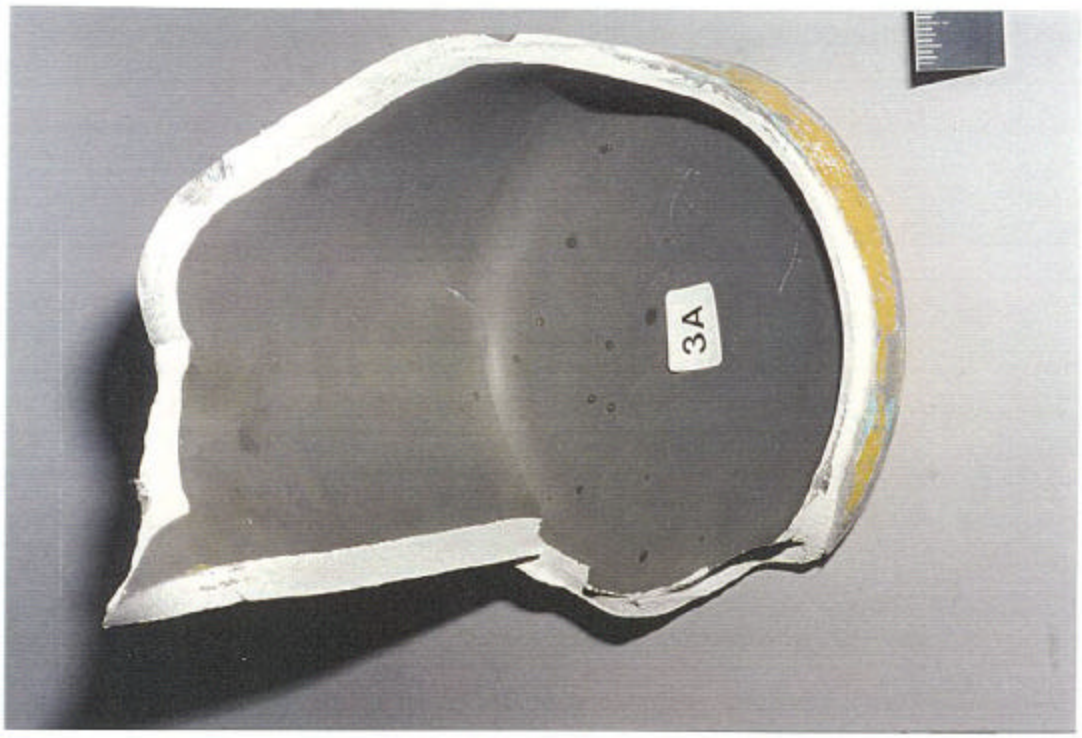

Photo ID: DC18234-R211

Photo ID: DC18234-R2E12

Photo ID: DC18234-R2E13

Photo ID: DC18234-R2E15

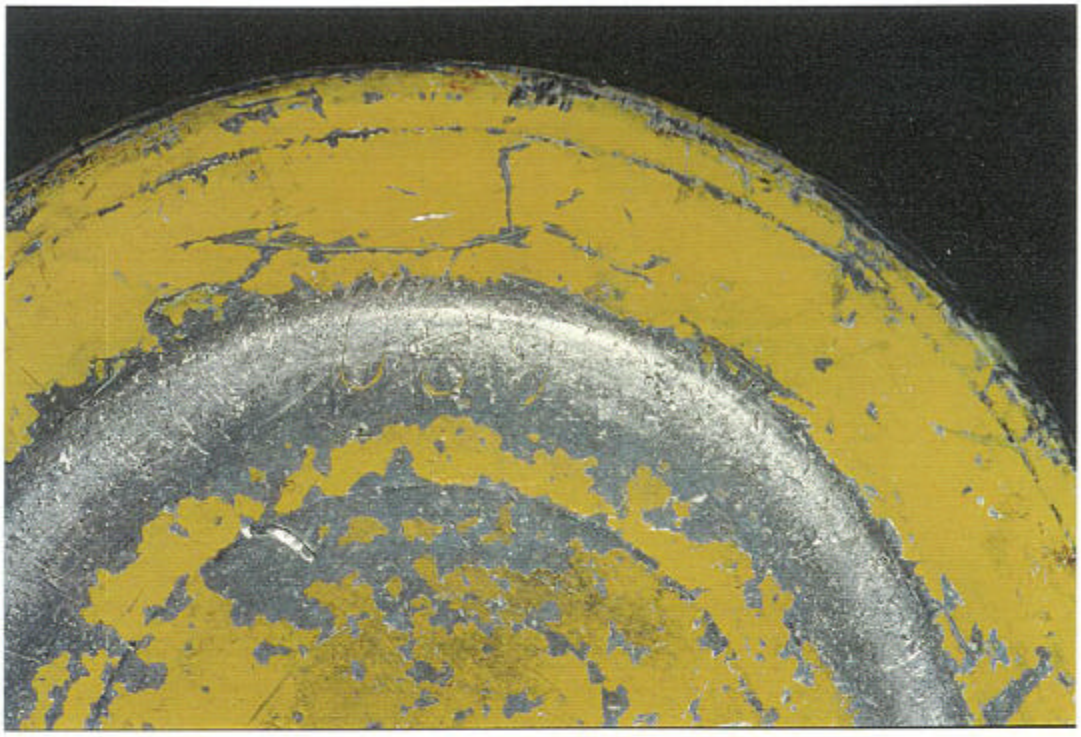

Photo ID: DC18234-R2E16

Photo ID: DC18234-R2E17

Photo ID: DC18234-R2E18

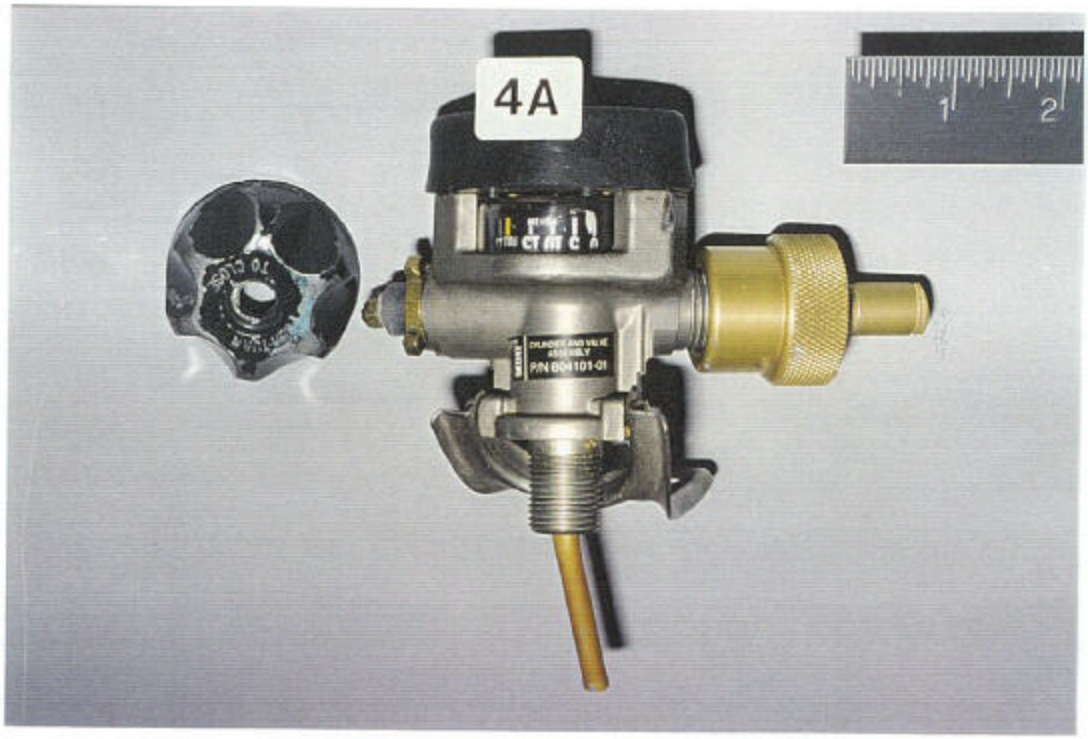

Photo ID: DC18234-R2E19

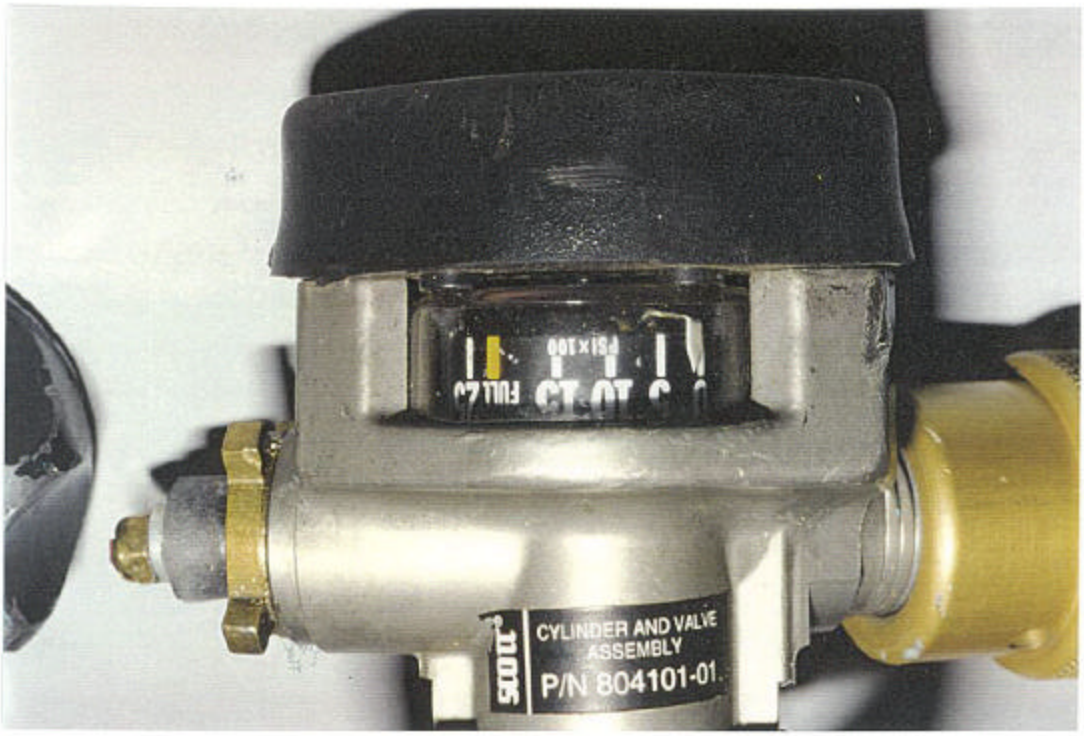

Photo ID: DC18234-R2E20

Photo ID: DC18234-R2E21

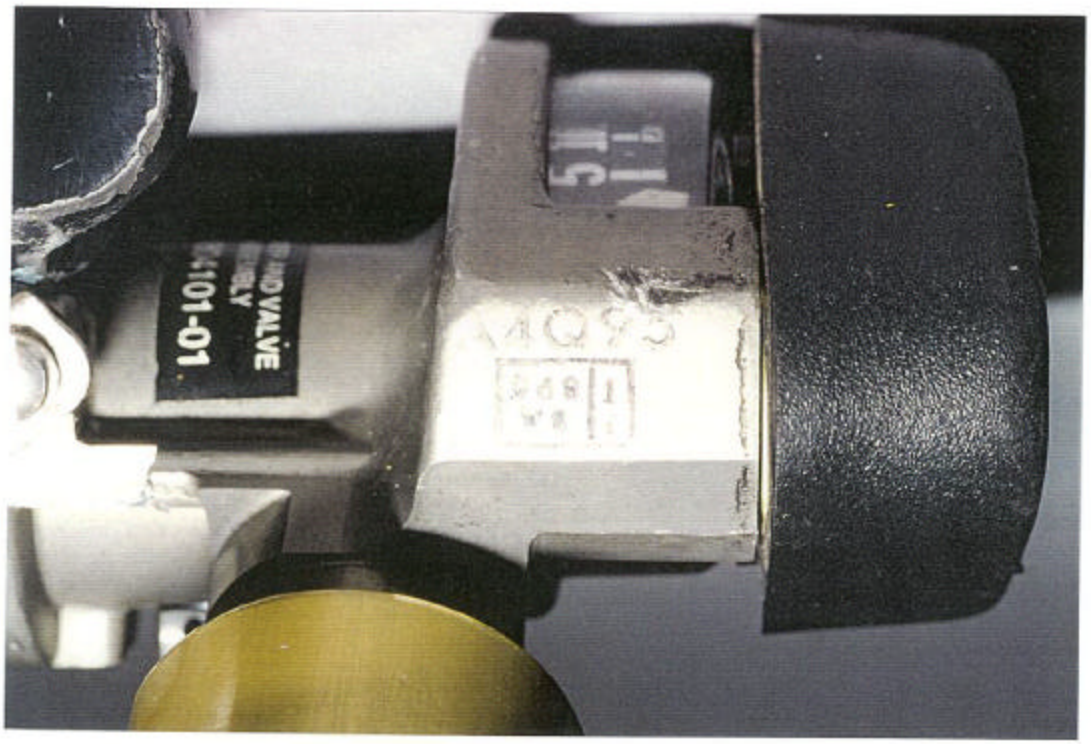

Photo ID: DC18234-R2E24

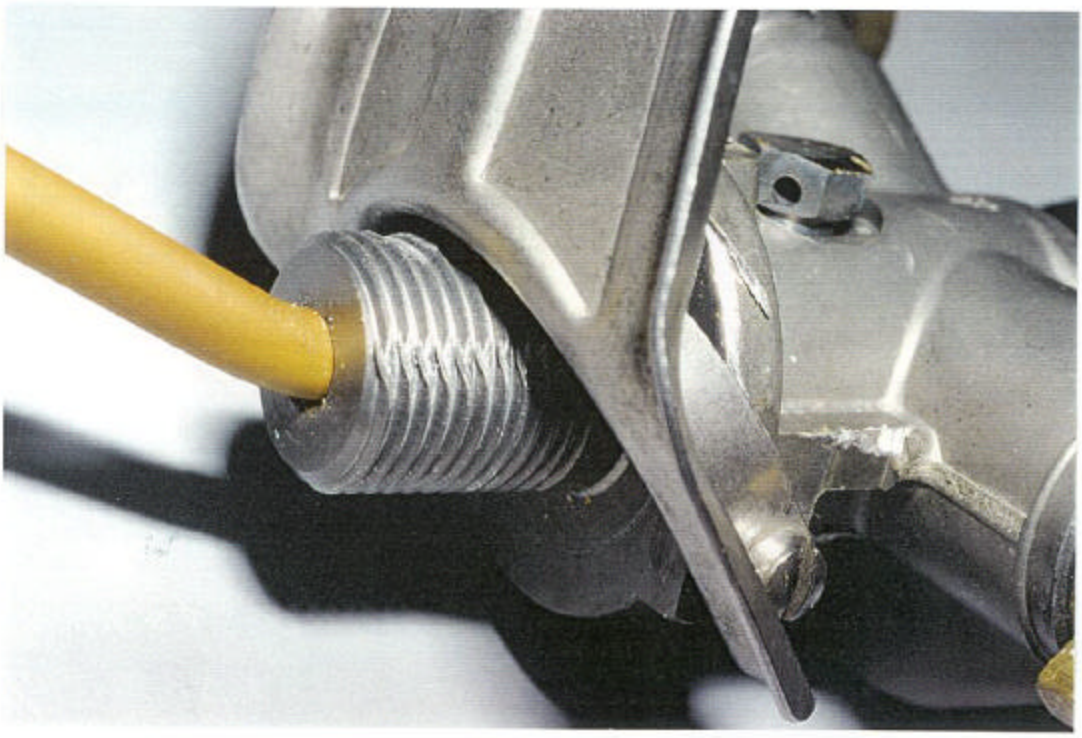

Photo ID: DC18234-R2E26